The Born versus Heisenberg Quantum-Vacuum controversy and beyond.

Luis Roso¹, Roberto Lera², Smrithan Ravichandran^{3,4}, Andrew Longman⁵, Calvin Z He^{3,4}, José Antonio Pérez-Hernández¹, Jon I Apiñaniz¹, Rohan Mahnot^{3,4}, Vicent Mateu⁶, Robert Fedosejevs⁷, and Wendell T Hill, III^{3,4,8}

- 1 Departamento de Física Aplicada, Universidad de Salamanca, 37008 Salamanca, Spain
- 2 Centro de Láseres Pulsados (CLPU), 37185 Villamayor, Salamanca, Spain
- 3 Joint Quantum Institute, University of Maryland, College Park, MD 20742, USA
- 4 Institute for Physical Science and Technology, University of Maryland, College Park, MD 20742, USA
- 5 Lawrence Livermore National Laboratory, Livermore, CA 94550, USA
- 6 Departamento de Física Fundamental, Universidad de Salamanca, 37008 Salamanca, Spain
- 7 Electrical and Computer Engineering, University of Alberta, Edmonton, Alberta T6G 2V4, Canada
- 8 Department of Physics, University of Maryland, College Park, MD 20742, USA

Corresponding author email: roso@usal.es

Abstract

Photon-photon collisions, as one of the fundamental processes in quantum physics, have attracted a lot of attention. However, most effort has been focused on photons energetic enough to create particle-antiparticle pairs. The low energy limit - e.g., optical photons - has attracted less attention because of their extremely low collision cross section. By optical photons we mean UV, visible and infrared, although the cutting edge of extreme lasers is in the near infrared. The Schwinger critical field for pair generation seems not possible, at least directly, with the current laser technology. This often is considered as a problem, but we view this as an asset; the near impossibility of pair production via photon-photon scattering in the infrared is a perfect scenario to study virtual pairs that characterize Dirac's quantum vacuum. Moreover, it is remarkable that this scenario of photon-photon collisions was already studied in the 1930s by two of the fathers of Quantum Mechanics, among others, at the dawn of this theory. In their respective papers, however, Born and Heisenberg arrived to different conclusions regarding the birefringence of vacuum. This controversy is still an open question that will be solved soon, we hope, with upcoming experiments. Here, we discuss a possible photon-photon collision experiment with extreme lasers, and will show that it can provide measurable effects, allowing fundamental information about the essence of Quantum Electrodynamics and its Lagrangian to be extracted. A possible experimental scenario with two ultra-intense pulses for detecting photon-photon scattering is analyzed. This would need a high-precision measurement, with control of temporal and spatial jitter, and noise. We conclude that such an experiment is barely feasible at 10²³ W/cm² (today's intensity record) and very promising at 10²⁴ W/cm².

Keywords: quantum vacuum, nonlinear QED, photon-photon scattering, extreme laser intensity

1.- Introduction

There is no doubt that Quantum Electrodynamics (QED) is one of the most successful theories, if not the most successful theory developed so far in quantum physics. It predicts experimental measurements with extraordinary precision and is the paradigm of what a theory must be. However, in the logical evolution of science one must seek the limits of a theory and test it against new information and with new experimental tools when they become available. One of those extraordinary tools is the laser and particularly laser pulses focused to extreme intensities. It is well known that with the Chirped Pulse Amplification (CPA) technique discovered by Donna Strickland and Gerard Mourou [1, 2] and subsequently developed during the past four decades, it is possible to generate intensities of 10²³ W/cm² [3]; this record is likely to be broken in a near future due to the enormous effort being expended to develop multi-Petawatt lasers with a goal of reaching the 0.1 Exawatt frontier. The present availability and future expectations of such extreme lasers, working in the near-infrared range, allows the design of new experiments to explore QED predictions in a nonlinear region in the absence of pair creation with lowenergy photons. Getting information on the deep study of matter using just the vacuum might seem contradictory. However, we should consider that vacuum is not really empty but is full of virtual particle antiparticle pairs. It is of fundamental relevance to study such pairs while they are virtual, which is best done today with infrared lasers. The world's laser community now has the "perfect tool" around which to design experiments at very low energies (compared with the electron rest energy), that will be complementary to the high-energy experimentation performed at big particle accelerators [4] and intermediate photon energies performed at Free-Electron Lasers (FELs) [5].

A priori it might seem that all is understood in this low energy limit, however there are two surprises:

- The first is the existence of two theories, one proposed by Born in 1934 and another proposed by Heisenberg in 1936, which give contradictory results. While the latter is now considered the lowest-order nonlinear term of the QED model, there are so far no experiments that support one or the other. Now, almost a century later since their presentation, this may be possible with ultraintense, infrared pulses.
- The second is an exploration of the quantum vacuum, that might give information and/or set limits on certain types of theorized dark matter particles. This is possible because infrared photons explore a region of the quantum vacuum where such dark matter might produce a measurable effect that could modify the first nonlinear QED term. This can be a tool to study dark matter form an alternative point of view.

Unfortunately, experiments to probe the quantum vacuum are not at all easy. A possible scenario to analyze scattered photons from the collision of two ultra-intense pulses is presented. While our approach would employ two infrared lasers (of the same frequency) there is another, ongoing two-frequency approach [6]. This is an experiment, currently in progress in Hamburg's European XFEL, where one of its X-ray beams, with an ultraprecise polarization [7], crosses the beam of a

focused petawatt-class laser [5]. The infrared laser produces a very small polarization rotation of the X-ray beam. The future success of this experiment requires an ultraprecise X-ray polarization rotation measurement.

2.- The 1934-1936 unsolved controversy on Quantum Electrodynamics

The precision of QED is astonishing in all situations in which it has been tested that includes a large variety of experiments. However, there are gaps, -- specific experimental configurations where it has not been tested, like the one in the context of the present project. We refer to this as a regime of very low energy photon-photon collisions, i.e., collisions between infrared photons. It is noteworthy that the very low energy photon-photon collision scenario was studied during the 1930s by two of the fathers of Quantum Mechanics, at the very dawn of this theory.

In 1936 Werner Heisenberg and Hans Euler [8] published in Zeitschrift für Physik a study based on the analysis of the Dirac equation, which had been published just a few years earlier. Two years prior to the Heisenberg-Euler paper, Max Born and Leopold Infeld [9] published a study based on the electron selfenergy in Proc. Royal Society London, which led to their Lagrangian governing photon-photon collisions [10]. This was a coincidence of historical relevance. The conflict arises at the moment one realizes that these two contributions to the study of photon-photon scattering reached contradictory conclusions. The difference is fundamental; while the Heisenberg-Euler (HE) result indicates the vacuum is birefringent, the Born-Infeld (BI) model suggests the vacuum acts as an isotropic medium. In spite of that, the physics community surprisingly never considered this controversy as relevant, at least up until now. Why is this controversy not widely known? Perhaps because of the hegemony of the Heisenberg-Euler model, which is often considered as the first-order correction QED model. It should be noted that the discrepancy appears only in the nonlinear terms, while most of the experimental measurements involving QED rarely, if ever, go beyond the linear situation where the two approaches agree.

It is widely accepted that the QED Lagrangian accounting for photon-photon coupling in the optical region has to be based on the only two possible covariant terms, $\mathcal{F} = \epsilon_0 (\mathbf{E}^2 - \mathbf{c}^2 \mathbf{B}^2)/2$ and $\mathcal{G} = \epsilon_0 (\mathbf{E} \cdot \mathbf{c} \mathbf{B})$. Thus, one can write it in a general way as, $\mathcal{L}_{\gamma\gamma} = \mathcal{L}_0 + \mathcal{L}_{NL}$ where the photon-photon Lagrangian $\mathcal{L}_{\gamma\gamma}$ has a linear term $\mathcal{L}_0 = \mathcal{F}$ that is very well known from Maxwell equations and Quantum Mechanics' early times. This term by itself is not able to account for photon-photon scattering. We are interested in the optical region, so we can restrict ourselves to the limit where the photon energy is much smaller than the electron mass ($\hbar\omega \ll m_e c^2$), otherwise conventional mass terms must be added to the Lagrangian.

There are many possibilities for the nonlinear effective Lagrangian \mathcal{L}_{NL} . The only restriction is to build combinations of the \mathcal{F} and \mathcal{G} terms, since they are the

only possible covariant choices. Working at the first non-linear order (the order we are interested in), there are three possible combinations,

$$\mathcal{L}_{\gamma\gamma} = \mathcal{F} + \xi_{\parallel} \mathcal{F}^2 + \xi_{\perp} \mathcal{G}^2 + \xi_* \mathcal{F} \mathcal{G}$$
 (1)

The key point for the discussion we want to convey here is that the Lagrangian is based on three coupling parameters ξ_{\parallel} , ξ_{\perp} , and ξ_{*} . The first non-vanishing order information on the photon-photon coupling is going to be found through these three parameters. The reason for using the subindex parallel in ξ_{\parallel} as well as the subindex perpendicular in ξ_{\perp} will be apparent in a moment. The analysis of the third coupling parameter, ξ_* , will be neglected in this chapter because it breaks the invariance under spatial reflections or time reversal [11] and QED must be invariant under these transformations. Addition of this term might be relevant in the future, once the experiment defined here indicates the possibility of such extra QED terms.

As stated earlier, the lack of consensus on the value of the nonlinear coefficients is the motivation for this chapter. Heisenberg and Euler [8] showed the instability of the Dirac vacuum for high fields based on this Lagrangian with the coupling constants,

$$\xi_{\parallel}^{\text{HE}} = \frac{8}{45} \alpha^2 \frac{\hbar^3}{m_e^4 c^5} = 6.7 \times 10^{24} \frac{\text{cm}^3}{\text{J}}$$
 (2a)

$$\xi_{\parallel}^{HE} = \frac{8}{45} \alpha^2 \frac{\hbar^3}{m_e^4 c^5} = 6.7 \times 10^{24} \frac{\text{cm}^3}{\text{J}}$$

$$\xi_{\perp}^{HE} = \frac{7}{4} \xi_{\parallel}^{HE} = \frac{14}{45} \alpha^2 \frac{\hbar^3}{m_e^4 c^5} = 11.7 \times 10^{24} \frac{\text{cm}^3}{\text{J}}$$
(2a)

This value ξ_{\parallel}^{HE} can be considered a reference of the coupling strength. Obviously $\xi_{*}=0$ in the Heisenberg-Euler formulation. The difference in the values of ξ_{\parallel}^{HE} and ξ_{\perp}^{HE} is the origin of vacuum birefringence, predicted by the Heisenberg-Euler (HE) model but not confirmed experimentally yet, although an experiment at European XFEL (X-Ray Free Electron Laser) in Hamburg is expected to answer this question soon using an X-ray probe of ultrahigh precision [7, 6].

Similar nonlinear effects should also occur with super-strong magnetic fields [12, 13, 14]. Perhaps the most sensitive and precision lab-based polarimetry measurements have been done in the optical region by the PVLAS collaboration [15] although they are not yet able to either confirm or rule out the birefringence that the Heisenberg-Euler model predicts.

The Heisenberg-Euler model coupling constants of Eq. (2) are the values considered in most of the literature, sometimes as the only ones compatible with QED. However, they are not the only ones possible. Born-Infeld, on the contrary, did not calculate a value for the coupling constants but rather proposed a linear relation between these coefficients, $\xi_{\perp}^{BI} = \xi_{\parallel}^{BI}$ [11]. Considering the whole line suggested by Born and Infeld (BI), what is more remarkable is that if this model is correct, the vacuum will not be birefringent, at least not birefringent by the couplings possible inside the particle physics Standard Model.

3.- Beyond the Standard Model

It is well accepted that the Standard Model is incomplete. There are indications of physics Beyond the Standard Model (BSM) in the form of new interactions and new particles. Some of the latter could be thought of as "dark matter" [16], that is, massive stable particles that interact gravitationally in the usual way, but do not interact - or do so in a very feeble way - with photons. We will assume as a working hypothesis they do interact, as suggested by existing models. The study of dark matter is of utmost importance as it seems to constitute 85% of the total matter in the universe. The evidence for dark matter is only indirect, through the observation of galaxy rotation curves that cannot be explained with the observed visible matter. Since dark-matter particles interact so weakly, finding them is challenging and so far they have escaped direct detection. Not having appropriate detectors, one can make advantage of the quantum paradigm and gather indirect evidence of their existence as virtual states (that is, propagating modes within Feynman diagrams). This is a usual strategy in particle physics, although it is normally applied in searches of particles too heavy to be produced. In our case, box-diagrams for photon-photon scattering in which charged dark-matter particles circulate, interfere coherently with the electron-loop contribution, thus affecting the numerical value of the effective Lagrangian (assuming their mass is higher than the energies involved in the experiment), or simply changing the cross section (if the mass is comparable or smaller than the energy). Other diagrams can be also present that will modify the effective Lagrangian too. This affects not only to dark-matter, but to any other particle that is hard to detect, for instance (but not limited to) axionlike particles (ALP) [15, 17]. Therefore, an experimental study of photon-photon scattering in the infrared domain can yield a lot of valuable information not only on which model is correct (HE or BI) but also on whether or not some kinds of dark matter indeed exist.

The BI versus HE historical controversy is based uniquely on the effect of the electron-positron pairs. Since the electrons (and its antiparticle, the positron) are the charged particles with the smallest mass they are expected to be the responsible for vacuum polarization. Heavier particles, as muons or pions (let alone protons), will have a negligible effect as the effect scales inversely as the fourth power of the mass [18]. The lightest known particle of all, the neutrino (conjectured by Wolfgang Pauli in 1930), does not interact with electromagnetic fields. For these reasons the study has to be reduced to electron-positron pairs. The controversy was triggered by the interpretation of the electrons and positrons on the grounds of the Dirac equation. The discrepancy between the Heisenberg-Euler Lagrangian, and other Lagrangians, such as the Born-Infeld, is a basic fundamental problem that has not been properly considered for many decades. Better knowledge could be key to a better understanding of some of the present-day questions that the Standard Model cannot address. A direct optical measurement of these coefficients would be of great interest. Moreover, the coupling is going to be different for pseudoscalar ALP (coupling with two photons through $\mathbf{E} \cdot c\mathbf{B}$), scalar ALP (coupling through \mathbf{E}^2 c²B²), as well as for other hypothetical BSM particles. A clean and precise determination of the coupling terms is of paramount importance, and would provide valuable data.

Using a phenomenological nonlinear Lagrangian, it is possible to write it in a form similar to Eq. (1),

$$\mathcal{L}_{\gamma\gamma} = \mathcal{F} + (\xi_{\parallel} + \Delta \xi_{\parallel}) \,\mathcal{F}^2 + (\xi_{\perp} + \Delta \xi_{\perp}) \,\mathcal{G}^2 \tag{3}$$

where $\Delta \xi_{\parallel}$ and $\Delta \xi_{\perp}$ are the possible corrections due to dark matter. Fortunately, different kinds of dark particles can result in different variations of these coupling coefficients. For example, scalar axions would result in a nonzero $\Delta \xi_{\parallel}$ and $\Delta \xi_{\perp} = 0$, while pseudoscalar axions would give nonzero $\Delta \xi_{\perp}$ and $\Delta \xi_{\parallel} = 0$. Other possible conjectured mini or millicharged particles would result in different ratios $\Delta \xi_{\perp}/\Delta \xi_{\parallel}$ of these two dark-matter correction effective coefficients. The dimensionless coefficient multiplying the (charge/mass)⁴ scale factor of the Lagrangian term in $\Delta \xi_{\parallel}$ or in $\Delta \xi_{\perp}$ depends on the spin of the hypothetical particle. For this reason it is important to design experiments that can clearly differentiate between parallel and perpendicular components. More information on this can be found in a previous book of this series [19].

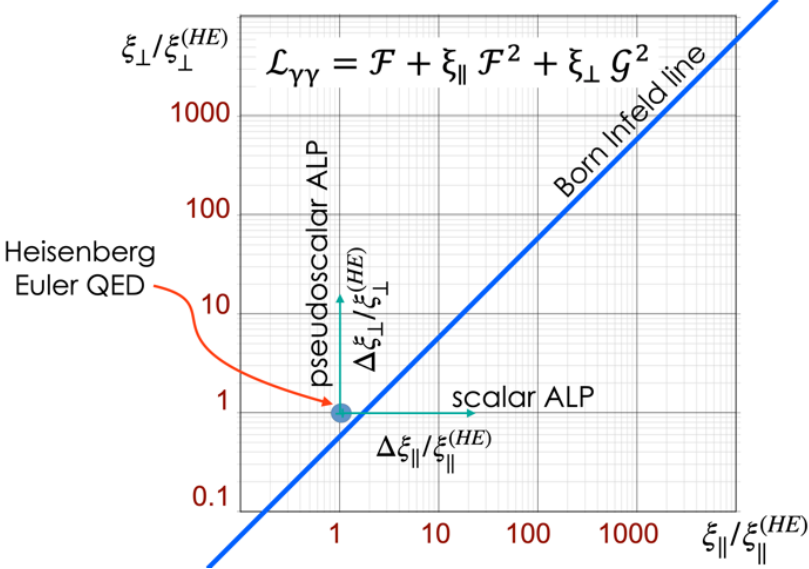


Figure 1. Configuration space of these two coupling coefficients appearing in the nonlinear Lagrangian $\mathcal{L}_{\gamma\gamma}$. For simplicity we used the axes $\xi_{\parallel}/\xi_{\parallel}^{HE}$ and $\xi_{\perp}/\xi_{\perp}^{HE}$, referring to the HE values. BI model predicts a line not intersecting the HE point, illustrating the discrepancy between the two theories. The addition of BSM particles could change the effective Lagrangian coupling parameters. While the QED point is the one predicted by HE, and the BI line is the bisector (representing no birefringence), the segments $\Delta \xi_{\parallel}/\xi_{\parallel}^{HE}$ and $\Delta \xi_{\perp}/\xi_{\perp}^{HE}$ have been depicted arbitrarily. Other sorts of millicharged hypothetical particles would result in corrections in different directions depending of their spin.

Fig. 1 shows this effective Lagrangian configuration space. For simplicity, the figure axes indicate the relative couplings, $\xi_{\parallel}/\xi_{\parallel}^{HE}$ (parallel) and $\xi_{\perp}/\xi_{\perp}^{HE}$ (perpendicular). The big dot at (1,1) indicates the HE point, and the thick line the BI line. Observe that the HE dot does not lie on the BI line, evidencing the discrepancy between both models. Addition of BSM particles can add extra terms to the effective Lagrangian coupling coefficients, $\Delta \xi_{\parallel}$ and $\Delta \xi_{\perp}$, causing a deviation in the configuration space from the HE model. Their values are not yet known, but the direction of deviation can be understood on the basis of the kind of particles we

are looking for. For example, pseudoscalar ALP would correspond only to $\Delta \xi_{\parallel}$ (and $\Delta \xi_{\parallel}$ =0), while scalar ALP would correspond only to $\Delta \xi_{\parallel}$ (and $\Delta \xi_{\perp}$ = 0). The arrows for the two kinds of ALP are shown in Fig. 1, although the length of the arrows has been arbitrarily selected. The length of these arrows, if nonzero, would be a clear evidence of such particles and of their properties, in a future laser-laser collision experiment. Other kinds of dark matter candidates will generate a correction in a different direction. For example, hypothetical spin 1/2 millicharged particles will have a correction along a line of slope 1 (similarly to the BI model, due to the spin 1/2 electron).

4.- Photon-photon scattering

Scattering of light by light [20] or, in other words, photon-photon collision, has received a lot of interest in the past as well at present. However, most of the physics seems to be related to photon-photon collisions at center-of-mass energies close to the the electron-positron pair mass to study such pair generation [21] or at even higher center of mass energies to produce muon-antimuon pairs [22] or to explore new unexplored high energy resonances [23] at the high energy frontier allowed at CERN LHC or other big particle accelerator systems available. The differential cross section for scattering of light by light has been studied in detail [24] for many decades and for many photon-energy ranges.

Besides this high energy scenario there is also the opposite one, the very low energy frontier. In the limit $\hbar\omega \ll mc^2$, i.e., photon energies ($\hbar\omega$) much smaller than the electron mass (mc^2). The photon-photon cross section decays abruptly as ω^6 . In this limit, the total photon-photon scattering cross section (integrated over all the sphere) and averaged for unpolarized photons is given by [25]

$$\sigma_{\gamma\gamma\to\gamma\gamma} = \frac{973}{10125 \,\pi} \, \frac{\alpha^4 \hbar^2}{m^2 c^2} \left(\frac{\hbar \omega}{mc^2}\right)^6 \tag{4}$$

where α is the fine structure constant. The laser photon energy $\hbar\omega$ has to be considered in the center of momentum frame (i.e., a frame in which both colliding photons have the same energy). This expression can be rewritten in more practical units, $\sigma_{\gamma\gamma-\gamma\gamma}[cm^2] = 0.73 \ 10^{-65} \ (\hbar\omega \ [eV])^6$, considering the cross section in cm² and the photon energy in eV. This means that for one of the most widely used type of CPA laser, the Titanium:Sapphire laser, which has photons with energies around 1.55 eV (we say around because of the large bandwidth of these lasers), the cross section may drop to values of 10^{-64} cm² (see Fig. 2). For this reason, the collision of optical photons has been disregarded for many decades. Now, with the availability of ultrahigh intensities [3], it seems to be the right time to reconsider this experimental situation.

Although it may seem that the most interesting scenario is the creation of new particles, basically electron-positron pairs, the situation of very small photon energies is very attractive because it interrogates the "true" vacuum. By true

vacuum we mean the vacuum far from the appearance of real pairs. After the introduction of Dirac's equation to describe the relativistic electron, it is clear that the vacuum is full of virtual particle-antiparticle pairs. The analysis of these virtual pairs can be done with lasers. This is relevant because it relates to one of the basic principles of quantum mechanics, but it is also interesting because it opens an alternative way to explore dark matter. From a more philosophical view point, it is curious that we seek getting information from nothing, from the vacuum. The quantum vacuum is a fabulous tool that does not require real particles to get new information (a very attractive feature for studying dark matter).

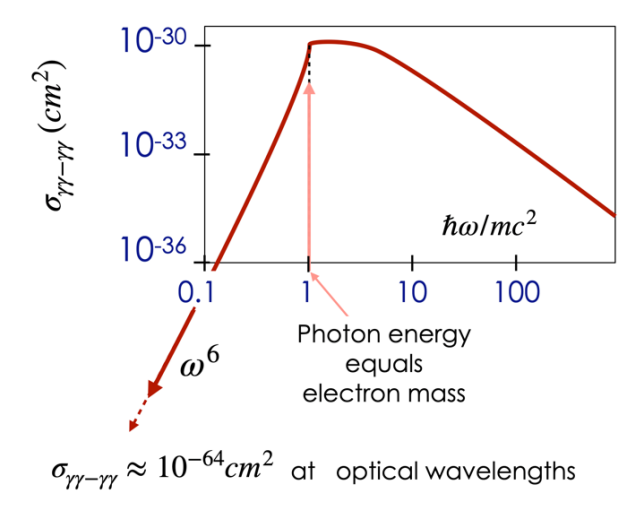


Figure 2. Schematic plot of the photon-photon head-on collision cross section. This value is approximate for non polarized photons. For parallel polarizations the cross section is slightly higher and for perpendicular polarizations is a bit smaller. This difference is due to the different coupling mechanisms that will be apparent later on this chapter.

The controversy between Heisenberg and Born as well as the study of different kinds of dark matter can now (or in a near future) be solved by conducting a specific experiment using ultraintense lasers. Extreme lasers are needed due to the extremely low cross-sectional area at infrared wavelengths. Let us analyze how to perform a realistic experiment, but before that, we need to stablish a QED-optics connection via the vacuum refractive index.

5.- Quantum Optical Kerr effect in the optical region

As indicated before, we are going to work well below the pair formation limit because on the one hand the laser frequency is much smaller than the electron mass ($\hbar\omega \ll m_e c^2$) and on the other hand the field amplitude is well below the Schwinger critical field (E $\ll E_{crit} \sim 1.32 \times 10^{16} \text{ V/cm}$) [20]. Therefore, real pair creation is avoided, in principle. Later we will comment on certain side effects that could induce real pair creation. Thus, the entire discussion is related to virtual pairs. Just to give a naïve but intuitive interpretation of the physics to be considered, we may say that ordinary vacuum is not completely empty, but full of virtual electron-positron pairs. It is not a contradiction to quantum mechanics to consider that these pairs exist, provided that they exist just for a short time. The incertitude of the energy is twice the electron mass and the corresponding implication of the Heisenberg uncertainty principle, $\Delta E \Delta t \geq \hbar/2$, $\Delta E = 2 m_e c^2 \sim 1$ MeV being the

excess of energy needed to generate the pair, and Δt the time allowed for this energy mismatch according to the Heisenberg uncertainty principle. This time happens to be very small, as expected, with $\Delta t \sim 10^{-22}$ seconds. However, with a conveniently large electric field these virtual pairs can live a bit longer because the field moves the electron and the positron in opposite directions. The fact that this Δt grows a little bit indicates a polarization in the quantum vacuum that translates in a small but nonzero nonlinear refractive index. This is just a simplified explanation. The correct way to link this with the refractive index has been described in several papers for different situations. One of the most clear and convincing has been presented by [11] considering this effect as a nonlinear refractive index. The consideration of vacuum as a material with an intensity-dependent refractive index is the link between QED and optics and will be very useful.

It is well known that, in most optical materials, as soon as the intensity increases, the refractive index is affected by a nonlinear term that changes with the intensity of the radiation that passes through it. For the quantum vacuum we can do the same and write the vacuum refractive index as $n(I)=n_l+n_2I,$ where n_l indicates the linear part of the refractive index (obviously $n_l=1$ for the vacuum) and n_2 indicates the nonlinear term. In this chapter we will measure n_2 in units of cm²/W and the intensity in W/cm², and the product will be dimensionless, as it should be. As the intensity increases, higher order nonlinearities appear for all materials and will appear for vacuum, too. For our purpose, and due to the available laser intensities currently or in the foreseeable future in operation or in construction, the approximation of considering just the first term, n_2I , is clearly sufficient.

We can consider the nonlinear refractive index for the probe pulse at each point in space and time as proportional to the pump intensity at the same point and time. The nonlinear index is essentially instantaneous, at least compared to the time scales considered here (optical laser period, few femtoseconds), because the characteristic time corresponding to 1 MeV (the electron-positron pair mass) is of the order of 10^{-22} seconds. It has been shown that this coupling results in a change of the vacuum refractive index [11]. This is the key point of this work: a signature of the quantum vacuum that can be observed as a simple change in the refractive index and thus optical techniques can be applied. Obviously, this change is very small and such experiments have to be planned with great accuracy to be prepared to measure a very small (but observable) signal in a very noisy environment. It is relevant to observe that a convenient choice of the fields will result in the predominance of the \mathcal{F}^2 term, when the fields are parallel, or of the \mathcal{G}^2 term when the fields are perpendicular. Therefore, the coupling due to one or the other Lagrangian terms is distinguishable, provided that the fields have a well-defined geometry.

The nonlinear index is in fact a tensor as in any anisotropic optical material, thus depending on the polarization. In the BI model it reduces to a number, again as in isotropic optical materials. However, what is more important is that the refractive index n is directly linked to the coupling coefficients of the nonlinear effective Lagrangian.

It is well known that a plane wave (monochromatic or broadband) can't generate such nonlinear effects. Without entering in the complete discussion given by [4] it is possible to give an intuitive idea to study the meaning of these couplings by analyzing the nonlinear terms in the Lagrangian. In the case of a linearly polarized plane travelling wave, as schematically indicated in Fig. 3, the two covariant terms \mathcal{F} , and \mathcal{G} are going to be $\mathbf{E}^2 - \mathbf{B}^2 = \mathbf{E}_A^2 - \mathbf{B}_A^2 = 0$, and $\mathbf{E} \cdot c\mathbf{B} = 0$ (where we have used the relation $\mathbf{E}_A = c\mathbf{B}_A$ for the electric and magnetic field amplitudes). The same result would be obtained for circular or elliptical polarization, assuming that it is a purely traveling wave.

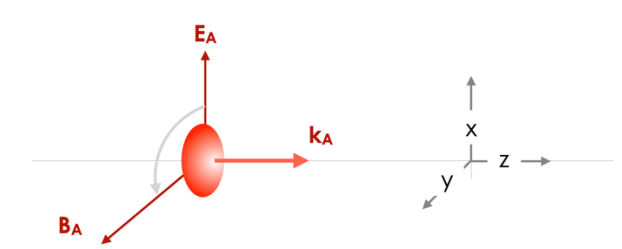


Figure 3.- In the case of a pure plane travelling wave, we have $\mathcal{F} = 0$, and G = 0. We label these fields with the subindex A, indicating the pump beam, because in the next sections we will introduce a probe beam. The present x, y, z axis notation is going to be the same for all this Chapter.

In the case of a tightly focused beam, the convergence can make these terms nonzero, albeit weak. The convergence is going to create a longitudinal electric and magnetic field, E_L and B_L, both propagating along the propagation direction z. The paraxial expression for these fields can be seen in [26]. Then we have $\mathbf{E} =$ $(E_A, 0, E_L)$ and $\mathbf{B} = (0, B_A, B_L)$, resulting in $\mathbf{E}^2 - c^2 \mathbf{B}^2 = E_A^2 + E_L^2 - c^2 B_A^2 - c^2 B_L^2 = 0$ (where we have used that $E_L = c B_L$), and $\mathbf{E} \cdot c \mathbf{B} = E_L c B_L$. Therefore, at focus, a single laser may create a nonzero quantum vacuum effect. This effect is associated with the longitudinal components existing at focus to preserve the $\nabla \cdot \mathbf{E} = 0$ and $\nabla \cdot \mathbf{B} = 0$ constrains. Obviously the effect is relatively small. It is well known that for a Gaussian pulse (TEM₀₀), the longitudinal field is zero on-axis and has its maximum at a distance from the axis of about 70 percent of the waist, therefore its contribution will not be too relevant.

Adding a second laser not as intense as the first one, it is possible to work in a pump-probe configuration. Having this in mind, we identify two completely different pump-probe configurations that represent two limiting situations. In Section 6, we will analyze the case of counterpropagating waves and in Section 7 the case of beams crossing at a right angle.

6.- Counterpropagating beams

Let's consider first the case of two counterpropagating lasers [27] (see Fig. 4). It can be shown that that in such a pump-probe configuration the n₂ nonlinear refractive index in the HE model is given by [11]

$$n_{2\parallel}^{HE} = 0.888 \times 10^{-33} \text{ cm}^2/\text{W}$$
 (5a)
 $n_{2\perp}^{HE} = 1.555 \times 10^{-33} \text{ cm}^2/\text{W}$ (5b)

$$n_{2\perp}^{HE} = 1.555 \times 10^{-33} \text{ cm}^2/\text{W}$$
 (5b)

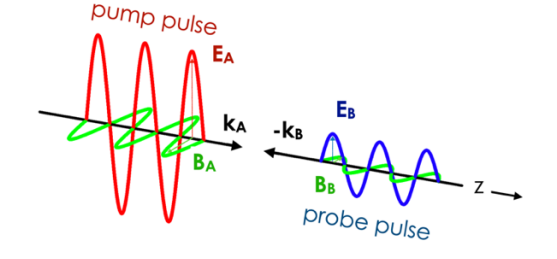


Figure 4. In Section 6 we study the case where the two propagation vectors are along the z-axis and counterpropagating. The pump will move as z-ct while the probe will move as z+ct. There are two cases of possible polarizations that have to be described.

In terms of the pump and probe configuration we are interested in, this means that the pump modifies the vacuum so that the probe, depending on its polarization, sees the $n_{2\parallel}$ nonlinearity if pump and probe electric fields are parallel and sees the $n_{2\perp}$ nonlinearity if pump and probe electric fields are perpendicular. In a general polarization case, the index will be in between these two values according to the projections in perpendicular and parallel components. We are interested in the design of an experiment that maximizes the difference between these two components, and ideally measures $n_{2\parallel}$ and $n_{2\perp}$ separately. The nonlinear coefficients scale as ξ_{\parallel} and ξ_{\perp} . The nonlinear refractive index assuming the HE theory can be used as a well-stablished reference, thus in the general case $n_{2\parallel}=n_{2\parallel}^{HE}\,\xi_{\parallel}/\xi_{\parallel}^{HE}$, and $n_{2\perp}=n_{2\perp}^{HE}\,\xi_{\perp}/\xi_{\perp}^{HE}$. In fact, we can refer to any effective model using these two ratios $\xi_{\parallel}/\xi_{\parallel}^{HE}$ and $\xi_{\perp}/\xi_{\perp}^{HE}$. The nonlinear refractive index is therefore proportional to these coupling coefficients. This makes the n_2 nonlinearity a perfect link between QED and optics.

We consider a pump-probe beam configuration. The suffix A will refer to the pump pulse and the suffix B to the probe. The probe has to be intense in order to have a high number of scattered photons, although it is always much weaker that the pump. All relevant quantum vacuum effects will be caused by the pump. To keep a constant notation of axes, the pump will move in the positive z direction, i.e., as z-ct. Because the signal we are looking for is the scattering of the probe photons, we have to minimize other sources of scattering/diffraction of the probe. Therefore, as indicated in [27], we choose a probe with a relatively wide waist, and a very good TEM_{00} structure. The shape of the pump pulse is not so relevant, provided it arrives to an extreme intensity.

For counterpropagating beams with parallel polarizations, Fig. 5a, $\mathbf{E}^2 - \mathbf{c}^2 \, \mathbf{B}^2 = (E_A + E_B)^2 - \mathbf{c}^2 \, (B_A + B_B)^2 = 4 \, E_A E_B$ because both the electric and the magnetic fields contribute to \mathcal{F}^2 . E_A and E_A (= c E_A) indicate positively defined electric and magnetic field amplitudes the pump beam, moving with z-ct. E_B and E_A and E_B indicate the probe beam positively defined amplitudes, moving as z+ct. Obviously, c $\mathbf{E} \cdot \mathbf{B} = 0$, and there is no contribution to the \mathcal{G}^2 term of the Lagrangian. The parallelism occurs between \mathbf{E}_A and \mathbf{E}_B and between \mathbf{E}_A and \mathbf{E}_B and the same time. This is why we refer this case as parallel.

Analogously, for counterpropagating beams with perpendicular polarizations, Fig. 5b, one has $\mathbf{E}^2 - \mathbf{c}^2 \ \mathbf{B}^2 = 0$, and $\mathbf{c} \ \mathbf{E} \cdot \mathbf{B} = 2 \mathbf{E}_A \mathbf{E}_B$ because both the electric and magnetic fields contribute to \mathcal{G} . The perpendicularity occurs between \mathbf{E}_A and \mathbf{E}_B and between \mathbf{B}_A and \mathbf{B}_B at the same time (this is relevant to remember when

comparing with tilted beams). Intermediate polarizations will couple via a combination of these two limiting cases. Therefore, for counterpropagating beams, all the possible information comes from the study of the two combinations of pump and probe polarizations.

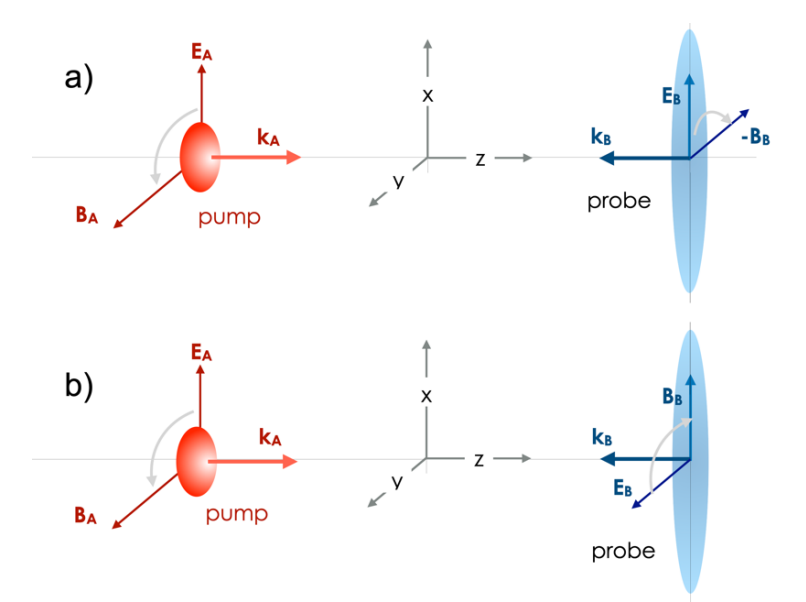


Figure 5.- Nonlinearity contributions for the two possible field polarization configurations in the case of counterpropagating pulses: a) corresponds to pump-probe parallel polarization, giving E^2-c^2 $B^2=4$ E_A E_B and $E\cdot cB=0$, and therefore the with these polarizations the fields couple only via the ξ_\parallel term; b) corresponds to pump-probe perpendicular polarization E^2-c^2 $B^2=0$, and $E\cdot c$ $B=2E_A$ E_B , and therefore these fields couple only via the ξ_\perp term of the Lagrangian. E_A and E_B indicate the positively defined electric field amplitudes of the pump and the probe beam respectively. B_A and B_B indicate the respective magnetic field amplitudes. They are all positively defined, with the sign explicitly indicated. The ordered vectors. E, B, and z form in all cases a right-handed orthogonal set.

Using counterpropagating fields is the best scenario to maximize the \mathcal{F}^2 and \mathcal{G}^2 Lagrangian terms. However, it has some technical difficulties because one laser can enter the amplifiers of the other if the alignment is too good. The experimental difficulties can be reduced with a configuration with the pump and probe beams at an angle. Therefore we will discuss later also the case of beams crossing perpendicularly.

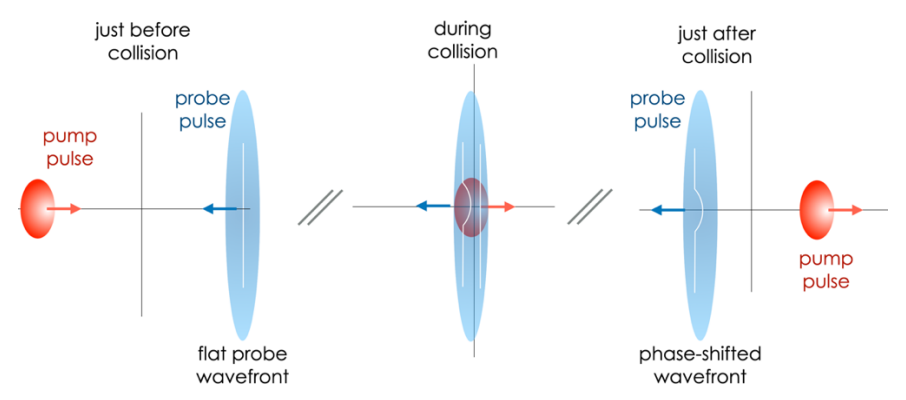


Figure 6.- Schematic representation of the head on collision. The probe has to cover the entirety of the focused pump to sample the phase change when the field has its maximum intensity.

The interaction between probe and pump pulses is indicated schematically in Fig. 6. The probe has a well-defined phase wavefront, planar near its waist. When the pulses cross each other, the quantum vacuum coupling introduces a phase shift. After the interaction, this phase shift will generate a diffraction of the probe beam, and this diffraction is what we are going to measure. This diffraction is caused by photon-photon collisions. In order to keep momentum conservation, a photon of the pump has to be scattered also. However this second photon is not observable due to the extreme and tightly focused pump.

Because we are interested in a configuration where the probe waist is relatively large, its Rayleigh length will be very long and, along the interaction region, it will have almost planar phase surfaces. It is reasonable therefore to consider just ray propagation for the probe, and calculate the phase shift due to the nonlinear term induced by the pump. As discussed in our previous paper [27], we recommend for such kind of experiments a tight pump focus and a wide waist probe with a very high optical quality. Although the probe peak intensity is not required to be so extreme, the needed optical quality and wide waist makes it challenging to prepare such probe pulses. The advantage of a wide waist is that all the quantum nonlinearities happen inside a region that is much smaller than the probe Rayleigh length. In this case we can consider (just very close to the probe waist) the probe wavefronts and calculate locally their phase considering probe rays.

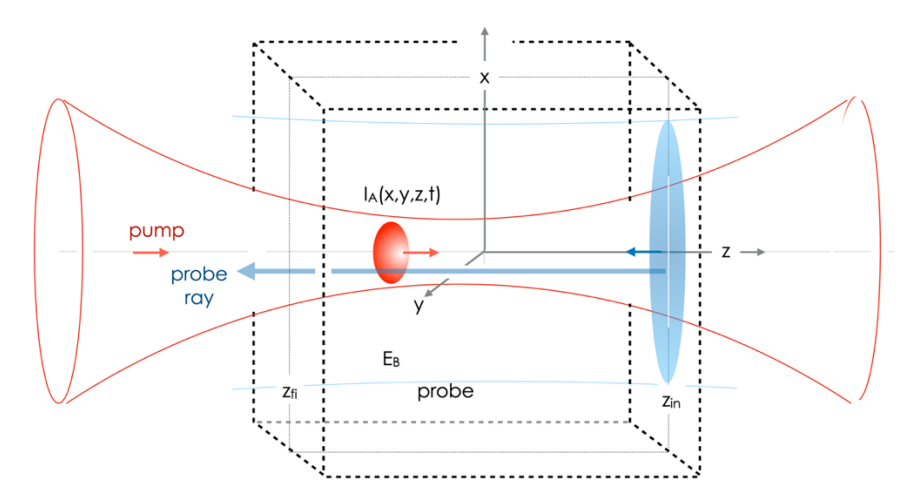


Figure 7. Ray modelling for the counterpropagating case. The phase shift calculation procedure considers individual probe rays in a region between two values of z (z_{in} , z initial, and z_{fi} , z final) that lie inside the probe Rayleigh length. Numerical integration to see quantum vacuum effects can be restricted to the dashed cube depicted.

For an accurate description of the pump interaction (see Fig. 7) it is enough to consider the probe propagation inside a medium with a refractive index given by n_2I_A , where n_2 is a constant parameter depending of the laser configuration and $I_A(x,y,z,t)$ is the time-dependent pump intensity. This can be time consuming and will give no information on the contributions relevant for the quantum vacuum nonlinearities. Such a computation has to be done before doing such a demanding experiment for a fine determination of the nonlinearities that will imply a fine

determination of the Lagrangian coupling parameters. However, the experimental scenario allows multiple choices of pump and probe laser geometries, detector positioning, light scattering, and many more effects. In order to optimize this, a simplified model, such as the one to be described, can be of interest to allow a realistic first approximation of the experimental scenario.

We are going to consider probe waists of 16 μ m or more (20 wavelengths or more). When the probe waist is so large, we can describe it near the focus as a plane wavefront. We know from the beginning that the influence of the quantum vacuum is going to be very small and can be accounted for as a minor phase shift. Therefore, it is enough to consider probe rays. In this situation the probe Rayleigh length is very large and there is the possibility to consider such a pulse as rays moving exactly along the z-axis. The general equation for each one of these probe rays is, $z + ct = ct_0$, x=constant, y=constant, where t_0 indicates the time where this element of the ray crosses the z=0 plane (the waist). We calculate the phase gained by each of the probe rays (at each time) due to the pump beam modification of the vacuum,

$$\phi(x, y, t_0) = k_B \int_{z_{in}}^{z_{fin}} n(x, y, z, t_0 - z/c) dz =.$$

$$= k_B (z_{fin} - z_{in}) + k_B \Delta \phi(y, z, t_0)$$
(6)

where the first term is $k_B(z_{fin}-z_{in})$ the optical (linear) path between the two points. The second term, $\Delta \varphi(x,y,t_0)$, is the one accounting for the vacuum nonlinearities and can be expressed as,

$$\Delta \phi(x, y, t_0) = k_B \int_{z_{in}}^{z_{fin}} n_2 I_A(x, y, z, t_0 - z/c) dz$$
 (7)

 $I_A(x,y,z,t_0-z/c)$ indicates the pump laser intensity along the probe ray (x constant, y constant, and $z-ct=ct_0$) being x and y the transverse coordinates for the probe ray considered and t_0 the time when the probe ray is at z=0, i.e., at the waist. Here we consider n_2 in general, depending of the field polarizations it can be $n_2 \parallel$, $n_{2\perp}$, or a combination of them.

The integration $region[z_{in}, z_{fi}]$ has to be smaller than the probe Rayleigh length in order to allow this ray approach. To continue with the development of the expression for the nonlinear phase shift is is necessary to guess the form of the pump beam near the focus.

$$I_{A}(x, y, z, t) = I_{0A} 2 \frac{\lambda_{A} N}{\pi \rho} J_{1} \left(\frac{\pi \rho}{\lambda_{A} N} \right) \exp \left(-2 \frac{(z - c(t + \Delta t))^{2}}{c^{2} \tau_{A}^{2}} \right)$$
(8)

Obviously $\rho^2 = x^2 + y^2$. With N=f/D being the focal number (D is the focusing parabola diameter and f its effective focal length). Δt indicates the pump-probe jitter. We assume that the probe is centered at the origin of coordinates at t=0 and that the pump will arrive to that focal point at a time Δt (a few periods at most). This expression describes the transverse dependence just at focus and is thus valid

only for very shot pulses. In any case a detailed description of the pump focus needs a numerical calculation that is beyond the scope of the present work. Including the explicit dependence of the pump intensity in the expression for the nonlinear phase shift, we get

$$\begin{split} & \Delta \varphi(x, y, t_0) = \\ & = k_B \int_{z_{in}}^{z_{fi}} n_2 I_{0A} \, 2 \, \frac{\lambda_B \, N}{\pi \, \rho} \, J_1 \left(\frac{\pi \, \rho}{\lambda_A \, N} \right) \, exp \left(-2 \frac{(2z - c(t_0 + \Delta t))^2}{c^2 \, \tau_A^2} \right) \, dz \end{split} \tag{9}$$

The integration is over the ray $z + ct = ct_0$, with y=constant and z=constant too (as we said, this is the equation of the ray, and t_0 indicates the time this phase plane crosses the x=0 plane). This is a useful expression to calculate the quantum vacuum phase shift, and generalization to other pump shape models is straightforward. The maximum shift is going to correspond to $t_0 = 0$. The integral for the phase shift can be extended to infinity if the pump focus is much tighter that the probe, as is the case we are considering. Eliminating the effect of Δt (no jitter), the shift will be

$$\Delta_{\text{max}} \phi(x, y, 0) = k_B n_2 I_{0A} 2 \frac{\lambda_B N}{\pi \rho} J_1 \left(\frac{\pi \rho}{\lambda_A N} \right) \int_{-\infty}^{+\infty} \exp \left(-2 \frac{(2z)^2}{c^2 \tau_A^2} \right) dz \quad (10)$$

$$\Delta_{\text{max}} \phi(0,0,0) = k_B n_2 I_{0A} \frac{\lambda_B}{\lambda_A} \sqrt{\frac{\pi}{8}} c \tau_A$$
 (11)

For the case we are interested in, $\lambda_A = \lambda_B = \lambda = 800$ nm, $k_B = 2\pi/\lambda_B$ and $\tau_A = 10$ cycles, this phase change is $\Delta_{max} \varphi \approx 4 \, 10^{-32} \, I_{0A}$ rad, with the pump intensity measured in W/cm². Therefore, the phase change is very small. Once we have the phase shift for each one of these wave-fronts we can calculate the effect of the probe wave. Just before the overlapping of the two fields, the probe field amplitude is $E_B(x,y,t)$ while after the interaction is $E_B(x,y,t)$ exp($i\Delta\varphi(x,y,t)$). Because the phase shift is much less than 2π , this can be approximated to be $E_B(x,y,t)(1+i\Delta\varphi(x,y,t))$, and we can write the field just after the nonlinear coupling as $E_B(x,y,t)+E_S(x,y,t)$ where $E_S(x,y,t)=i\Delta\varphi(x,y,t)$ $E_B(x,y,t)$ indicates the scattered term, the one that we have to measure. The measurement has to be carried out at a point in space far from the waist. Thus, we can apply the well-known Fraunhofer diffraction equations. In the far field, the unperturbed probe (without pump) will be

$$F_{B}(\zeta) = -\frac{i}{\lambda_{B}} \int_{0}^{\infty} 2 \pi \rho \, E_{B}(\rho) \, J_{0}(k_{B} \, \rho \, \zeta) d\rho \tag{12}$$

We label the fields at the observation plane by F and the fields near the focus by E, just for clarity of the notation. Both correspond to electric fields. Therefore, F^2 will indicate the intensity at the observation plane. ζ indicates the polar angle (we assume cylindrical symmetry). The quantum vacuum signal will be given by

$$F_{S}(\zeta) = -\frac{i}{\lambda_{B}} \int_{0}^{\infty} 2 \pi \rho \, E_{B}(\rho) \, i \, \Delta_{max} \phi(\rho) \, J_{0}(k_{B} \, \rho \, \zeta) d\rho \qquad (13)$$

where $\Delta_{max} \varphi(\rho)$ indicates the maximum dephasing given by the $\Delta_{max} \varphi(x, y, 0)$, for $\rho^2 = x^2 + y^2$. This is a reasonably simple expression to calculate the scattered light. The scattered intensity at a scattering angle ζ will be proportional to $|F_S(\zeta)|^2$.

While it is clear that the nonlinear effect is due to the pump and it is necessary to have a very intense pump, the influence of the probe is rarely considered although it is fundamental for a successful experiment. F_B indicates the probe beam propagation at large distances. Its diffraction (linear diffraction) has to be confined within a narrow cone -as narrow as possible- in order to avoid overlapping with the quantum vacuum signal (nonlinear diffraction) out of this cone. The lowest linear diffraction occurs with a perfect Gaussian, thus we impose having a probe with a good Gaussian shape, with very high optical quality and with a relatively large waist.

We assume a Gaussian probe beam B given by $E_B(\rho) = E_{0B} \exp(-\rho^2/w_B^2)$. Just to get a sense of how many photons per solid angle we have in the probe beam we can analytically calculate the propagation (nonperturbed propagation) of the probe beam close to the z-axis. We calculate the intensity on axis for a small solid angle, 1 deg², centered at the z-axis, we call this axial intensity along z, $I_{axial}(z)$ and the solid angle $d\Omega$. With w_B as the waist of beam B and I_B its the intensity at the waist, the probe intensity along the propagation axis will be expressed as, $I_{axial}(z) = I_B (\pi w_B^2 / z \lambda_B)^2$ and the surface corresponding to this solid angle is $z^2 d\Omega$. Therefore, $I_{axial}(z) z^2 d\Omega = I_B (\pi w_B^2 / \lambda_B)^2 d\Omega$. The fluence will be this expression multiplied by τ_B . Each Joule corresponds to 4 10¹⁸ photons, at 800 nm. Thus, the number of probe photons will be $n_{ph}=10^{18}~I_B~\tau_B~k_B^2~w_B^4d\Omega~$ photons per Joule per solid angle. In the case of I_B=10²⁰ W/cm², this is a very challenging requirement to obtain a a good Gaussian shape and will require a lot of filtering. Observe that 0.000305 sr correspond to one deg². Therefore, for w_B=20 wavelengths=16 μ m and for 30 fs pulse duration, this corresponds to n_{ph} = 3.7×10^{19} photons. The number 3.7 10^{19} photons per shot, for $I_B=10^{20}$ W/cm², arriving to the detector (on axis) for w_B=16 µm (20 wavelengths), for 30 fs pulse duration and a detector on axis covering one deg² solid angle, is going to be considered as a realistic reference for the comparisons presented. For other intensities, because the number of photons scales as the intensity, the value 10^{20} W/cm² can be a reasonable reference. This is the background we have to avoid.

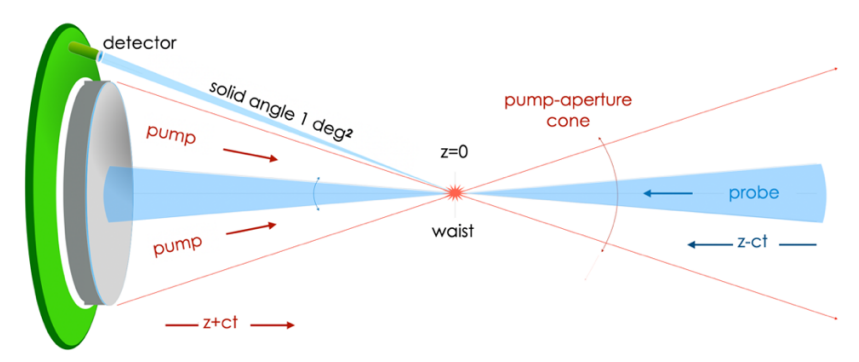


Figure 8. A possible setup for the counterpropagating case is shown in this figure. Due to the geometry, we can place a ring of detectors covering one, or a few degrees radially and all the circle, as shown in this scheme. However those detectors must be placed at an angle larger than

the pump aperture cone (given by the pump f-number). Because the probe has a large waist, its diffraction cone will be smaller than the pump aperture cone.

Fig. 8 shows a possible experimental setup. The two beams, pump and probe, are counterpropagating. The tight pump focus imposes a wide aperture cone. The probe detection has to be just outside of this pump aperture cone, and can be on a circle (green detection circle in the figure). Fig. 9 shows the log₁₀ of the number of scattered photons arriving to a detector covering a surface of one degree square versus the scattering angle. The figure corresponds to pump and probe of the same wavelength, 800 nm, and to a pump focus with f/3 focal number. Due to the pump aperture angle, the detection has to happen at angles greater than 0.17 rads. The angular region forbidden by this is shaded in blue in this figure. This is a problem for counterpropagating beams with a tight pump focus. Working at f/1.1 as in the world intensity record [3], the aperture of the pump would represent a fundamental difficulty to the placement of the scattered probe photons detectors. Because a short f-number corresponds to a wide focal cone. Observe that here the probe parameters are waist 16 μm and peak intensity 10²⁰ W/cm². For a detector placed at an angle of 0.2 rads out of the collinear axis (z-axis) Fig. 9 indicates that there are 0.01 scattered photons expected per deg² detection solid angle for a pump intensity of 10²³ W/cm² per shot, and one scattered photon per shot for a 10²⁴ W/cm² pump. Observe the scaling with the intensity. As we said [3], the pump intensity 10^{23} W/cm² can be considered as today's record; the intensity 10²⁴ W/cm² will be sooner or later a reality. These numbers are for a detector covering only one deg². We can consider a ring-shaped detection, i.e., a detector that covers a ring of one degree width. For this ring-shaped detector a few scattered photons are expected per shot when using the probe we considered (waist 16 µm, peak probe Gaussian shape with a peak intensity 10²⁰ W/cm²) for a pump intensity of 10²³ W/cm². Ramping up the simulations to intensities greater that 10²⁴ W/cm² can be questioned because other effects may be present, as radiation reaction or electron pair cascading, although for this kind of nonlinear vacuum experiments, an extremely high vacuum level is necessary.

The solid blue line in Fig. 9 indicates the probe beam linear diffraction cone (linear means without pump). It is a section of a parabola centered at angle zero (a Gaussian in log scale). The detection of the scattered photons inside the probe linear diffraction cone is impossible. Scattered photons out of this cone are represented by the red dashed lines in the figure. However, the pump focusing system also implies a forbidden cone (blue shadowed region) that is the space occupied by the pump focusing parabola (see Fig. 8).

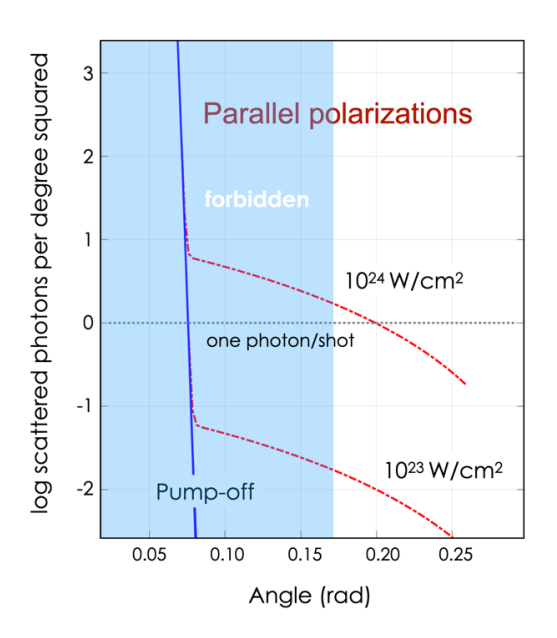


Figure 9. Log_{10} of the number of scattered photons per degree squared versus the scattering angle ζ for the case of an f/3 for the pump and w_B=16 µm for the probe, both at 800 nm. The solid (blue) curve corresponds to the linear case, i.e. without pump. The probe intensity at the center of the focus is 10²⁰ W/cm², the dashed (red) curves correspond to two different intensities of the pump. In this case, both fields overlap exactly at the focal spot. The number of photons has been calculated assuming a 1 deg² detector area. The figure corresponds to the parallel polarization case calculated with $n_{2\,\parallel}^{H\bar{E}}$, as a reference. Obviously, for the perpendicular case, $n_{2\perp}^{HE}$, simply multiply by the 7/4 factor. For other values of n₂, these numbers can be considered as a reference in order to depict the next figure. Observe the scaling of the number of scattered photons with the intensity squared.

With all these considerations we extract some conclusions on the possibility to detect the two coefficients of the effective Lagrangian introduced in Eq. (1). A complete analysis depends on many factors but it can be reasonable to consider that one photon per deg² per shot can be a threshold for detection (always with the the standard Gaussian probe with waist 16 µm and peak intensity of 10²⁰ W/cm²). If this is the case, for pump intensities of 10²⁴ W/cm² we must arrive to the Heisenberg-Euler point. This is indicated in Fig. 10, where the progressively darker blue regions indicate our estimation for the possibility to detect the Lagrangian coupling coefficients at this pump intensity level. We say that this is just an estimation because such an experiment would strongly depend on the noise sources. For the lack of space, we do not discuss here the noise sources that are very relevant for such a weak signal. A discussion can be found in [27]. Here we have considered the counterpropagating geometry and the refence number of one deg² square detector. With a detection ring, the solid angle covered can be increased by a factor to 100 or even 1000, but not more because of the quick dropping of the number of scattered photons with the scattering angle that can be seen in Fig. 9. Also, we have considered a probe with a peak intensity of 10²⁰ W/cm² and with a good Gaussian shape. Although this probe intensity does not seem extreme at first sight, it is extreme too due to the large waist and the requirement of a good optical quality and a Gaussian shape.

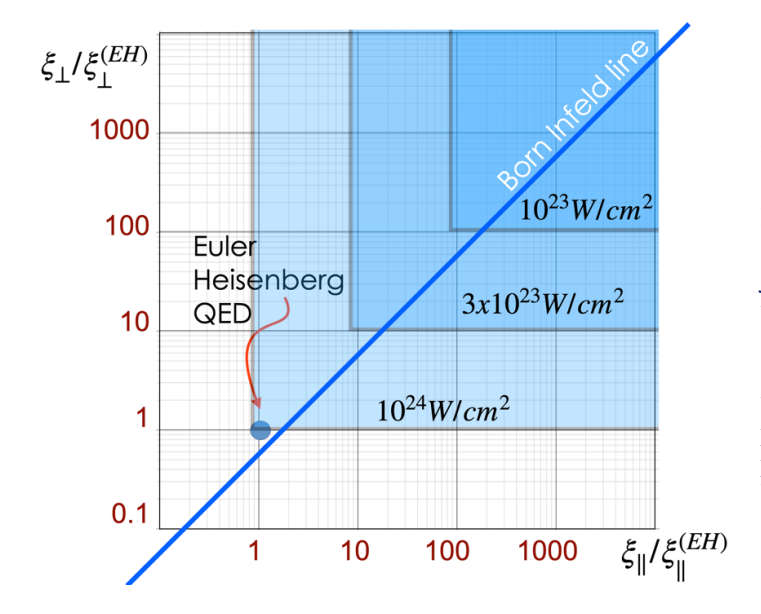


Figure 10. Possibility to observe the effective Lagrangian coefficients for different intensities. This is just an indication assuming that clear conclusions may appear at the detection level of one photon per deg² (for the standard Gaussian probe with waist $16 \mu m$ and peak intensity of 10^{20} W/cm²).

Let's comment briefly about the pump/probe jitter introduced in Eq. (9). For that it is better to move to a Gaussian description of the probe. Since the only relevant part of the nonlinear coupling happens close to the laser focus, it is a reasonable approach (open to improvement) to consider the pump as a Gaussian pulse with a waist w_A given by $w_A = 0.87 \lambda_A N$. Where λ_A is the pump central wavelength (800 nm for Ti:Sapphire lasers) and N indicates the focal number. In that case the pump Rayleigh length is $z_{RA} = \pi w_A^2/\lambda_A$. A very loose focus results in a peak intensity too low for the effects we are looking for. On the contrary, a very tight focusing helps to increase the peak intensity at the price of a strongly convergent beam that mixes up the different components of the electric field. This complicates a clean measurement of the parallel and perpendicular coupling coefficients. Probably, a good compromise is around N=3. For that case $w_A = 2.6 \, \lambda_A = 2.1 \, \mu m$, the Rayleigh length will be $z_{RA} = 17 \, \mu m$. These numbers are indicative of the size needed for the pump in order to cross the probe focus as a quasi-plane wave. This is only an approximation for the central part of the Airy focus, to prepare convenient scaling laws. If we call I_{0A} (z) the intensity of the central part (i.e., for $\rho = 0$) of the beam (axial) it is going to change with z as [27],

$$I_{0A}(z) = \frac{\pi^2 w_A^4}{\pi^2 w_A^4 (z) + z^2 \lambda_A^2} I_{0A}(0) = \frac{5.65 N^4 \lambda_A^2}{5.65 N^4 \lambda_A^2 + z^2} I_{0A}(0)$$
(14)

where we wrote the intensity in terms of the focal number. Expressing z in terms of the jitter time, $2z = c\Delta t$ (see Fig. 11), allows us to modify Eq. (10). Assuming that the relative jitter is smaller than the Rayleigh length of the probe, the nonlinear phase shift is going to be:

$$\begin{split} & \Delta_{max} \varphi \text{ (with jitter } \Delta t) = \\ & = k_B n_2 \frac{5.65 \text{ N}^4 \lambda_A^2}{5.65 \text{ N}^4 \lambda_A^2 + 0.25 \text{ c}^2 \Delta t^2} I_{0A}(0) \frac{\lambda_B}{\lambda_A} \sqrt{\frac{\pi}{8}} \text{ c } \tau_A \end{split} \tag{15}$$

This expression is of great experimental interest because it represents a characteristic Lorentzian shape of the dependence of the quantum vacuum signal

with the pulse delay time Δt between pump and probe. In an experiment where we need to get rid of an enormous noise-background, the knowledge of the signal dependence with the pulse delay is fundamental because the rest of the noise sources are not affected by a small pulse delay. Scaling laws like this one, do not seem very relevant in principle but for future experiments can be of paramount relevance to train artificial intelligence systems to detect patterns due to signal to noise specific scalings.

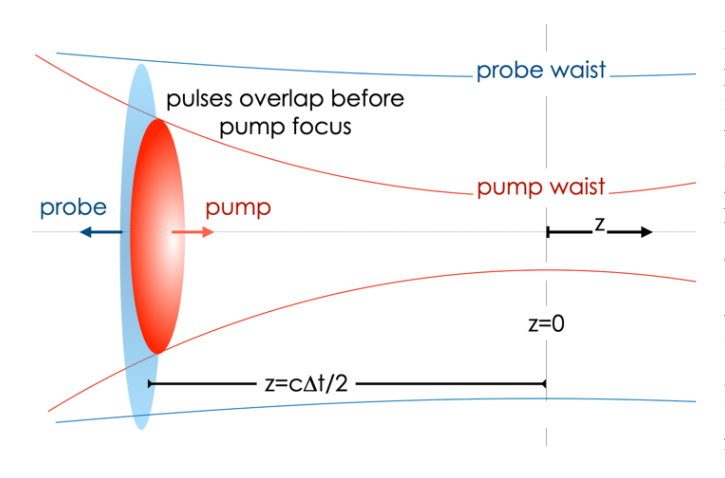


Figure 11. A jitter between pump and probe may result in an overlapping out of the waist. If Δt is the pump jitter (assuming the probe synchronized, perfectly then the overlapping will occur at a distance $z=c\Delta t/$ 2 from the waist. Therefore the overlap will occur at a lower pump intensity and at a wider pump waist, two factors that reduce the nonlinear scattering we are looking for.

7.- Crossing beams

Up to now we have only considered counterpropagating lasers. To avoid some of the problems generated by counterpropagating beams it is also possible to work with beams crossing at an arbitrary angle. In that case the n₂ nonlinearities, parallel and perpendicular, have to be modified. Although it is possible to develop models for any arbitrary angle, we restrict ourselves here to the case that both lasers cross at a right angle, in other words to the case where pump and probe wavevectors are perpendicular. To avoid confusion with the word perpendicular, used for polarizations, we would refer here to beams crossing at a right angle (see Fig.12).

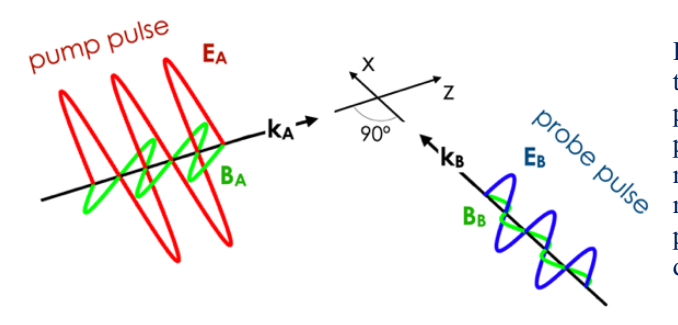


Figure 12. In Section 7 we study the case where where the two propagation vectors are crossing perpendicularly. The pump will move as z-ct while the probe will move as x-ct. All four cases of possible polarizations have to be described.

From this point on we will consider only a geometry where pump and probe propagate about different directions. In particular we will consider the pump moving towards the positive side of the the z-axis, with a wavevector \mathbf{k}_A =

 $(0,0,k_A)$, $k_A = 2\pi/\lambda_A$, being λ_A the pump pulse central wavelength. Therefore, the pump field propagation will be z-ct. And we will consider the probe moving towards the positive side of the the x-axis, with a wavevector $\mathbf{k}_B = (k_B, 0,0)$, $k_B = 2\pi/\lambda_B$, where λ_B is the probe pulse central wavelength. Therefore, the probe field propagation will be x-ct. We consider that both pulses are going to collide close the origin of coordinates (0,0,0).

Working with crossed beams, the problem of light from one beam entering the amplification chain of the other is totally avoided, and this is certainly beneficial from the experimental point of view, particularly if experiments with a high repetition rate have to designed due to the ultralow signal we expect to get. However, the quantum vacuum nonlinearity is reduced as the beams increase their relative angle. It can be shown [11] that the nonlinear terms change with the tilt angle between the pump and probe beams by a factor $\cos^4(\theta/2)$, where θ is the tilt angle between pump and probe, $\theta=0$ for counterpropagating and $\theta=\pi/2$ for the geometry to be described here. Therefore, at this $\theta=\pi/2$ tilt angle the nonlinearities are going to be reduced by a factor 4. In spite of this reduction, there can be other causes that favor such experiments at these angles (or at intermediate tilts). We will keep the notation $n_2/4$ in the following discussion and thus n_2 will indicate the nonlinearities for the counterpropagating case. Obviously there will be the two nonlinear indices n_2 and n_2 depending of the electric and magnetic fields polarizations.

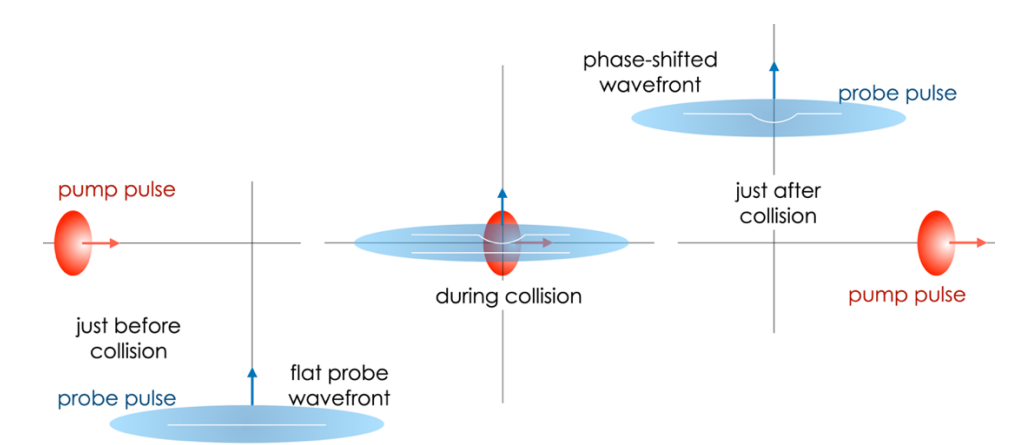


Figure 13. Schematic geometry of the pump-probe interaction described. We study the small phase shift that the quantum nonlinear effect introduces on the probe pulse after crossing a very intense pump pulse.

In this case the probe beam phase-shift is going to be produced in a collisional geometry as the one depicted in Fig. 13. We consider that the probe arrives with a flat optical phase (near its waists) and due to the interaction to the extreme field, it changes its phase by a small amount (much lower than one wavelength). This phase shifted wavefront will result in a diffracted probe beam.

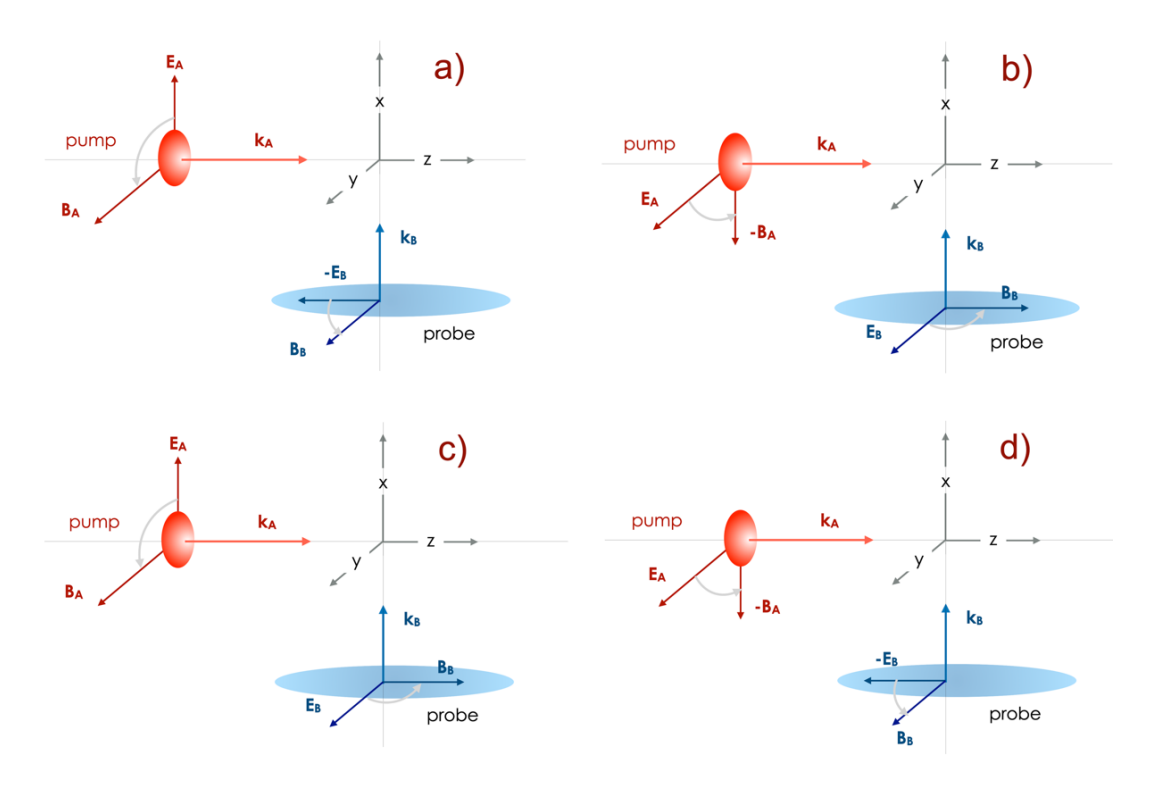


Figure 14. In this case of crossing beams there are four polarization configurations. Two of them (a and b) can be considered as parallel, or better longitudinal, because they "explore" the $\mathbf{E}^2 - \mathbf{c}^2 \mathbf{B}^2$ coupling, being $\mathbf{E} \cdot \mathbf{c} \mathbf{B} = 0$. The other two (c and d) can be considered as perpendicular, or better transverse, because they "explore" the $\mathbf{E} \cdot \mathbf{c} \mathbf{B}$ coupling, being $\mathbf{E}^2 - \mathbf{c}^2 \mathbf{B}^2 = 0$.

For the case of counterpropagating cases there were only two possibilities, perpendicular or parallel, as shown in Fig. 5. However, in the case of beams crossing at a right angle there are four basic configurations that are described in Fig. 14. While in the counterpropagating case it was possible to have pump and probe electric fields parallel and at the same time that pump and probe magnetic fields parallel too, in this case this is not possible. Fig. 14a corresponds to parallel pump and probe magnetic fields. The electric fields are perpendicular. In this case, the two nonlinear couplings in the Lagrangian are $\mathbf{E}^2 - c^2 \mathbf{B}^2 = -2 \mathbf{E}_{\mathbf{A}} \mathbf{E}_{\mathbf{B}}$ (observe that E=cB) and $\mathbf{E} \cdot c\mathbf{B} = 0$. Observe that in the case of parallel counterpropagating lasers shown in Fig. 5a the coupling is $\mathbf{E}^2 - c^2 \mathbf{B}^2 = 4 \mathbf{E}_{\mathbf{A}} \mathbf{E}_{\mathbf{B}}$. This is the reason why the coupling in this case is smaller than the coupling in the counterpropagating geometry. In the case of Fig. 14b the electric fields of pump and probe are parallel. The magnetic fields are perpendicular. Now the two nonlinear couplings in the Lagrangian are $\mathbf{E}^2 - \mathbf{c}^2 \mathbf{B}^2 = 2\mathbf{E}_A \mathbf{E}_B$ and $\mathbf{E} \cdot \mathbf{c} \mathbf{B} = 0$. Again, half of the value for counterpropagating parallel fields. Fig. 14c corresponds to one configuration where the pump and the probe electric fields are perpendicular and so are the magnetic fields. Therefore $\mathbf{E}^2 - \mathbf{c}^2 \mathbf{B}^2 = 0$, and $\mathbf{c} \mathbf{E} \cdot \mathbf{B} = \mathbf{E}_{\mathsf{A}} \mathbf{E}_{\mathsf{B}}$. Again, in the case of counterpropagating fields, shown in Fig. 5b, this contribution would have been E. $c\mathbf{B} = 2 E_A E_B$. It is therefore clear that the coupling is half of the counterpropagating coupling for perpendicular polarizations. The last possibility is presented in Fig. 14d, that corresponds to the perpendicular case too and where the couplings are $\mathbf{E}^2 - \mathbf{c}^2 \mathbf{B}^2 = 0$, and $\mathbf{E} \cdot \mathbf{c} \mathbf{B} = \mathbf{E}_{\mathbf{A}} \mathbf{E}_{\mathbf{B}}$. As we see, the terms ξ_{\parallel} and ξ_{\perp} correspond to parallel and perpendicular polarizations but in the sense explained here. These examples of basic reasoning can be very useful when designing experimental

configurations for such kind of experiments. As indicated before we omitted the influence of the longitudinal fields. For the loose focus of the probe this can be reasonable, but for a tightly focused pump such longitudinal effects can be of certain relevance.

In the case of crossing beams, we can also use the ray description introduced previously. Since we are interested in a configuration where the probe waist is relatively large, its Rayleigh length will be very long and along the interaction region it will have almost plane phase surfaces. It is reasonable therefore to consider just ray propagation-probe ray propagation- and calculate the phase shift due to the nonlinear term induced by the pump. As discussed in our previous paper we recommend for such kind of experiments a tight focus pump and a wide waist probe with a very high optical quality. Although the probe peak intensity won't be so extreme, the needed optical quality and wide waist makes it a challenge to prepare such probe pulses.

The advantage of a wide waist is that all the quantum nonlinearities happen inside a region that is much smaller that the probe Rayleigh length. In this case we can consider (just very close to the probe waist) probe wavefronts and calculate locally their phase considering probe rays.

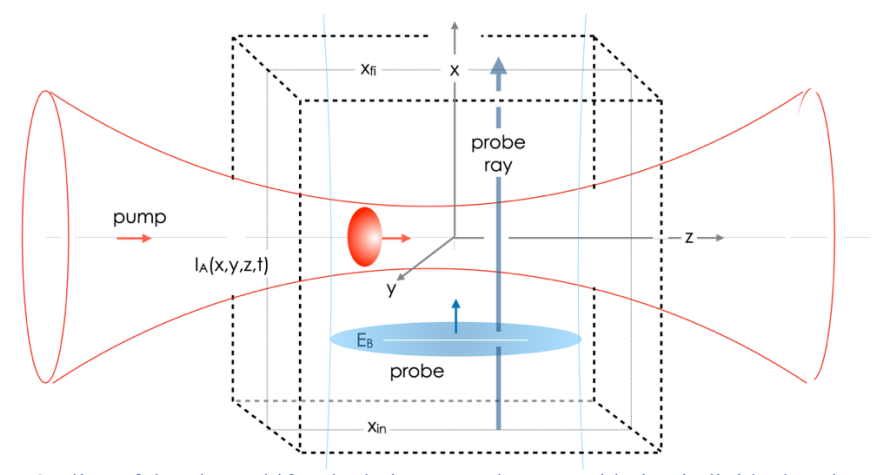


Figure 15. Outline of the phase shift calculation procedure, considering individual probe rays in a gion between two values of x (x_{in} , x initial, and x_{fi} , x final) that lie inside the probe Rayleigh length. umerical integration to see quantum vacuum effects can be restricted to the dashed cube depicted.

As indicated for the counterpropagating case, it is enough to consider the probe propagation inside a medium with a refractive index given by n_2I_A . A ray description is also valid. Fig. 15 is the evolution of Fig. 7 with the only change being that now the probe moves along x as x-ct.

If the probe waist is large enough, we can describe it near the focus as a plane wavefront. We know from the beginning that the influence is going to be very small and can be accounted for as a phase shift. Therefore, it is enough to consider probe rays. These are geometrical lines x-ct= constant, y=constant and z=constant, in a way similar to our approach to study the counterpropagating case.

The scheme of such interaction is given in Fig. 16. Because the probe waist is relatively wide in the interaction region, we describe it as a plane-wavefront. Before the collision the wavefront is a plane moving upwards in the figure. During the interaction with the pump, the quantum vacuum effect adds a phase in the regions where the pump intensity is high. After the collision this probe wavefront leaves the interaction region with a very small phase-shift according to the pump intensity it has passed through. All this happens inside the Rayleigh length of the probe. From this moment on, the quantum vacuum coupling is over and the wavefront propagates (diffracts) in the vacuum. This diffractive evolution can be accounted for using the well-know Fraunhofer diffraction model because the detectors are going to be placed at a distance from the collision point of the order of tens of centimeters or even meters (such long distance could also be useful for certain time gating techniques). In the case of positioning the detection devices close to the focus, the well-known Fresnel diffraction models have to be considered.

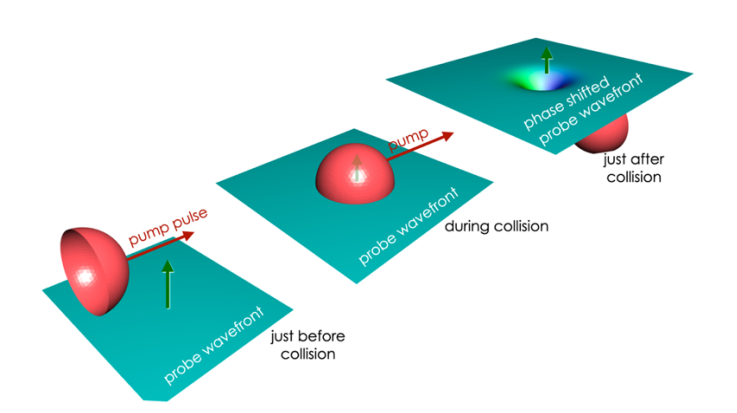


Figure 16. Schematic representation of a probe wavefront phase plane change. Before crossing the focus (left) the wavefront (blue) is a plane. During the interaction with the pump pulse (center) it acquires a phase shift proportional to the intensity the probe has "seen". After that we get a phase shifted wavefront (right).

As in the counterpropagating case, we are going to consider a probe waist of 16 μ m just to show the benefits for detection (this value can be considered a compromise between a very low diffraction probe and still possibility to arrive to relatively large probe intensities). In this situation the probe Rayleigh length is very big (\sim 1 millimeter) and there is the possibility to consider such pulse as rays. Rays moving exactly along the x-axis. The general equation for each one of these rays is, $x - ct = ct_0$, y= constant, z=constant. t_0 indicates the time where this element of the ray crosses the x=0 plane. The analogous to Eq. (7) for the nonlinear phase shift in this case is

$$\Delta \phi(y, z, t_0) = k_B \frac{n_2}{4} \int_{x_{in}}^{x_{fin}} I_A(x, y, z, x/c - t_0) dz$$
 (16)

This expression represents the phase shift of the ray moving along a line parallel to the x-axis, in the integration region that has to be smaller than the probe Rayleigh length in order to allow this ray approach.

To continue with the development of the expression for the nonlinear phase shift is is necessary to define the form of the pump beam near the focus. We introduce this analogously to what we did to arrive to Eq. (9). As defined previously, $\rho^2 = x^2 + y^2$, N=f/D is the focal number (D is the focusing parabola diameter and f its effective focal length), and Δt indicates the pump-probe jitter. We assume that the

probe is centered at the origin of coordinates at t=0 and thus the probe can arrive to be centered at that point at a time Δt (a few periods at most).

$$\Delta \phi(y, z, t) = \\ = k_{B} \frac{n_{2}}{4} \int_{x_{in}}^{x_{fi}} I_{0 A} 2 \frac{\lambda_{B} N}{\pi \rho} J_{1} \left(\frac{\pi \rho}{\lambda_{A} N} \right) \exp \left(-2 \frac{(z - c(t + \Delta t))^{2}}{c^{2} \tau_{A}^{2}} \right) dx$$
(17)

This expression is analogous to Eq. (9), with the obvious difference that now we have integrated over the ray $x - ct = ct_0$ constant, with y and z constant too (this is the equation of the ray, and t_0 indicates the time this phase plane crosses the x=0 plane). A difficulty appears now, the integral over dx involves the ρ variable and therefore an expression as simple as the indicated in Eq. (11) can not be worked out.

Thus, to get an insight of the important features of this interaction it is better to use a Gaussian description of the pump intensity near its waist, as we also did for the derivation of Eq. (14). Working with a Gaussian pump pulse characterized by a waist w_A given by $w_A = 0.87 \lambda_A N$, the pump intensity near the focus will be

$$I_{A}(x, y, z, t) = I_{0A} \exp\left(-2\frac{x^{2} + y^{2}}{w_{A}^{2}}\right) \exp\left(-2\frac{(z - c(t + \Delta t))^{2}}{c^{2} \tau_{A}^{2}}\right)$$
(18)

we can obtain enlightening equations for the nonlinear phase shift. The phase shift acquired by this probe ray we are considering will be

$$\Delta \phi(x, y, t_0) = k_B \frac{n_2}{4} I_{0A} \int_{x_{in}}^{x_{fi}} \exp\left(-2\frac{x^2 + y^2}{w_A^2}\right) \exp\left(-2\frac{(z - c(t + \Delta t))^2}{c^2 \tau_A^2}\right) dx$$
 (19)

Eq. (19) gives an analytical expression for the phase shift under these approximations. We can go one step further and considering that all the nonlinear interaction is between the $x=x_{in}$ and the $x=x_{fi}$ planes. Therefore, we can artificially extend the integral to $\pm\infty$

$$\Delta \phi(t) \approx k_B \frac{n_2}{4} I_{0A} \int_{+\infty}^{-\infty} \exp\left(-2 \frac{x^2 + y^2}{w_A^2}\right) \exp\left(-2 \frac{(z - x + ct_0)^2}{c^2 \tau_A^2}\right) dx$$
 (20)

and therefore,

$$\begin{split} \Delta \varphi(x,y,t_0) \\ \approx k_B \frac{n_2}{4} \; I_{0A} \exp \left(-2 \left(\frac{(w_A^2 + c^2 \tau_A^2)(c^2 \tau_A^2 y^2 + w_A^2 (z + ct_0)^2) + w_A^4 (z + ct_0)^2}{w_A^2 \; c^2 \tau_A^2 (w_A^2 + c^2 \tau_A^2)} \right) \right) \\ \sqrt{\frac{\pi \; w_A^2 c^2 \tau_A^2}{2 \; (w_A^2 + c^2 \tau_A^2)}} \end{split} \tag{21}$$

We neglected the jitter Δt for simplicity, adding it is straightforward. For $t_0 = 0$, we are considering the moment that the probe wavefront crosses the pump pulse

just at the waist. This will the case of maximum phase shift. Thus, the maximum shift for the ray x-ct, y, z is given by

$$\Delta \phi_{\text{max}}(y, z, 0)$$

$$\approx k_{\text{B}} \frac{n_{2}}{4} I_{0\text{A}} \exp\left(-2 \frac{(w_{\text{A}}^{2} + c^{2} \tau_{\text{A}}^{2})(c^{2} \tau_{\text{A}}^{2} y^{2} + w_{\text{A}}^{2} z^{2}) + w_{\text{A}}^{4} z^{2}}{w_{\text{A}}^{2} c^{2} \tau_{\text{A}}^{2} (w_{\text{A}}^{2} + c^{2} \tau_{\text{A}}^{2})}\right) \sqrt{\frac{\pi w_{\text{A}}^{2} c^{2} \tau_{\text{A}}^{2}}{2 (w_{\text{A}}^{2} + c^{2} \tau_{\text{A}}^{2})}}$$
(23)

This expression is important because indicates the dependence of the phase with the pump pulse shape. From approximate equations similar to this, a lot of information to design an optimized experiment can be obtained.

Among the results we can extract from this equation pertaining to the design of an experiment, we can study the optimized pump waist/length ratio. The equation for $\Delta \phi_{max}(y, z, 0)$ just obtained depends on two parameters that characterize the pump laser pulse, its waist w_A and its length $c \tau_A$. The relation between these two parameters is of fundamental importance. Considering that the central part of the pulse has a Gaussian form close to the focus and that it has symmetry of revolution (w_A is equal for x and for y) we can have a spheroidal shape (ellipsoid of revolution along the z-axis). It is well known that there are three kinds of spheroids: oblate (or disk shape), when c $\tau_A < w_A$; true spherical, when c $\tau_A = w_A$; and prolate (or cigar shape), when $c \tau_A > w_A$. Because the minimum, Fourier-transform limited, value of τ_A is determined by the laser bandwidth, it is possible to leave a residual chirp when compressing the pulse to produce a value of τ_A to be slightly bigger. Although this is seldom considered in the context of extreme fields, it would be also interesting to consider pulses without revolution symmetry, i.e. pulses where the waist w_A is different for the two transverse directions, $w_{Ax} \neq w_{Ay}$ [28]. These anisotropic Gaussian pulses could optimize the pump-probe overlapping in certain situations, although we are not going to consider them now.

Coming back to isotropic/spheroidal pulses, it is normal to refer the ratio of these two parameters as the eccentricity of the spheroid. The eccentricity ε is defined by $\varepsilon = c \tau_A/w_A$. Considering the ray crossing for the line z=0, y=0 and introducing the eccentricity parameter, Eq. (23) becomes

$$\Delta \phi_{\text{max}}(0,0,0) = k_{\text{B}} \frac{n_2}{4} I_{0\text{A}} \sqrt{\frac{\pi w_{\text{A}}^2 c^2 \tau_{\text{A}}^2}{2 (w_{\text{A}}^2 + c^2 \tau_{\text{A}}^2)}} = k_{\text{B}} I_{0\text{A}} \sqrt{\frac{\pi \varepsilon^2}{4 (1 + \varepsilon^2)}} c \tau_{\text{A}}$$
 (24)

Obviously, the maximum phase shift occurs when $c\tau_A$ goes to infinity, keeping the waist w_A constant, but this is artificial because the energy inside the pump pulse is going to be proportional to w_A^2 $c\tau_A$ (i.e. proportional to the volume of the spheroid) and increasing $c\tau_A$ while keeping I_{0A} constant would require more and more energy. It is more interesting to consider that experimentally adding a residual chirp to the pulse just distributes the energy. Thus, we can maximize the expression for $\Delta \varphi_{max}(0,0,0)$ with the constrain that w_A^2 $c\tau_A$ is kept constant. It is not difficult to see that the max dephasing $\Delta \varphi_{max}(0,0,0)$ happens for an eccentricity equal to $\epsilon = \sqrt{2}$, i.e. $c\tau_A = 1.41$ w_A . In this case Eq.(24) becomes

$$\Delta \phi_{\text{max}} \simeq 0.72 \text{ k}_{\text{B}} \text{ n}_2/4 \text{ I}_{0\text{A}} \text{ c}\tau_{\text{A}} \tag{25}$$

That gives the maximum value of the phase shift for a given pulse energy when the two lasers, of the same wavelength, cross at at $\pi/2$ angle. It is worth comparing this expression with Eq. (11) for counterpropagating lasers that can be simplified to $\Delta_{\rm max} \varphi = 0.63 \, \rm k_B n_2 I_{0A} \, c\tau_A$. As indicated before, n_2 corresponds to the counterpropagating case and may have two values according to the field's polarizations (parallel, $n_2 \parallel$, or perpendicular, $n_2 \perp$). We have explicitly written the $n_2/4$ factor in Eq. (25) to remind us of the $\pi/2$ angle of the two propagation vectors.

8.- Comparison between the two situations

We have analyzed the case of counterpropagating beams and the case where the two beams cross at a right angle. These can be considered as the two limiting cases. Obviously the copropagating case is not of interest. Besides a coefficient close to one, depending on the pulse configuration, there are two main differences that can be of fundamental relevance for the design of a quantum vacuum experiment. These differences are: the coupling factor, and the observation angle.

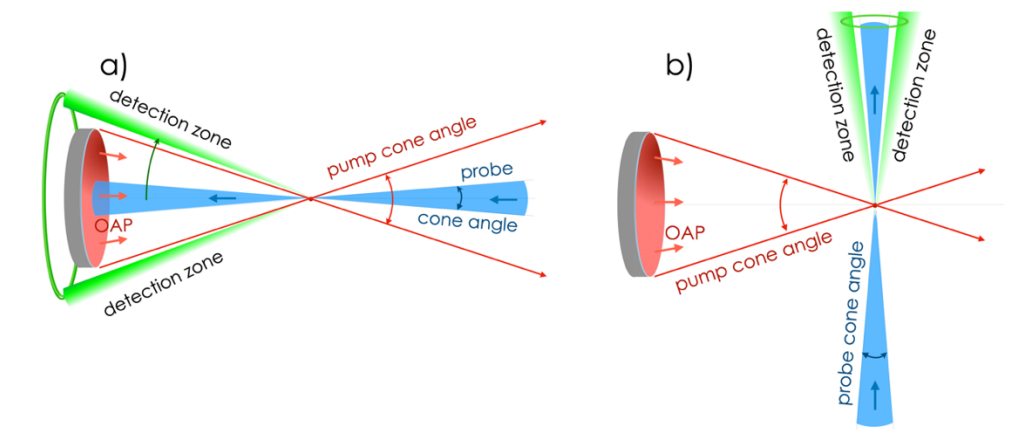


Figure 17. One relevant advantage of working with beams crossing is that the observation can be done at a small angle (a). However in the case of counter-propagating beams (b) the pump cone angle is a region avoided for detection because of the pump off-axis-paraboloidal (OAP) mirror used for the tight focusing of the pump. The tighter the focus, the bigger the pump cone angle, and this can be a major difficulty to work with focal numbers smaller than three. The scattered photon detection zone (or detection ring) is indicated in green in the figure.

By the coupling factor we refer to the $\cos^4(\theta/2)$ factor described in the previous Section, where θ is the tilt angle between the pump and the probe propagation directions. For beams crossing at a right angle $(\theta = \pi/2)$ this factor is 1/4 while for counterpropagating beams $(\theta = 0)$ this factor is one. Therefore any possible quantum vacuum signal is going to be four times bigger in the case of counterpropagating than in the case of crossing at a right angle. This seems a strong

argument in favor of working with counterpropagating beams. However there is a second fundamental difference.

The angle of observation of the scattered light is the second point to consider to decide which beam configuration is the most adequate. One relevant advantage of working with beams crossing is that the observation can be done at a small angle, as indicated in Fig. 17a. However, in the case of counterpropagating beams (Fig. 17b) the pump cone angle is a region avoided for detection because of the pump off-axis-paraboloidal (OAP) mirror used for the tight focusing of the pump. The tighter the focus, the bigger the pump cone angle, and this can be a major difficulty to work with focal numbers smaller than three. The detection zone (or detection ring) is indicated in green in the figure. A detection a few degrees closer to the probe axis can be fundamental because the scattered signal drops very quickly as the angle increases as can be see in the red dotted lines of Fig. 9. In this figure, the focal cone angle (f/3 in the figure) is the shaded region indicated as forbidden, and this forbidden cone happens only in the counterpropagating case. In the case of beams crossing at a right angle the detection can be as close as the probe diffraction allows. For this reason it is fundamental to have a probe with a Gaussian profile to minimize its linear diffraction.

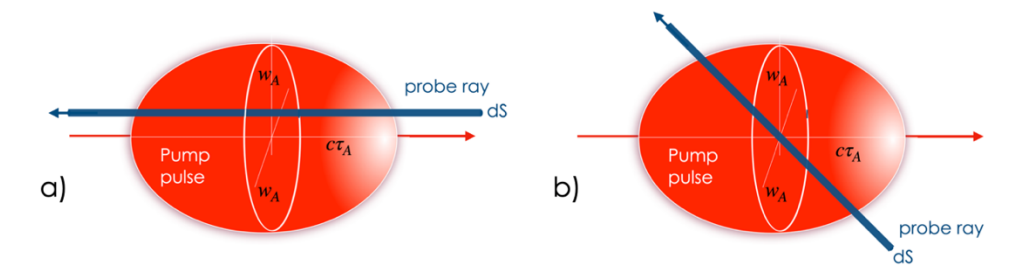


Figure 18. The quantum vacuum nonlinearity depends not exactly on the peak intensity but on the line integrated energy density "seen" by each differential pencil (probe ray). The red ellipses represent the pump pulse with its waist, w_A , and duration $c\tau_A$. The blue line represents the probe ray pencil of differential section dS that probes the vacuum nonlinearity. The phase shift acquired by this probe ray gives the fundamental information to calculate the nonlinear probe beam diffraction. Depending of the pump probe configuration the probe ray scans the pump pulse in a different way. a) corresponds to the path of the probe ray for counterpropagating fields (Section 6). b) corresponds to pump and probe pulses crossing at a right angle (Section 7). The pump-probe relative motion results in the effective scanning, along the pump pulse, shown in b).

9.- Scaling with linear density of energy

Observe that for the two geometries discussed, the phase increment is proportional (with a constant depending of the geometry but close to unity) to $k_B n_2 I_{0A} c\tau_A$, as shown in Eqs. (11) and (25) respectively. k_B is the probe wavenumber, the shorter the probe wavelength the higher the wavenumber, but the diffraction angle is also going to be smaller. All has to be considered when designing an experiment. n_2 is the nonlinear term to measure (parallel or perpendicular). And finally, we get $I_{0A} c\tau_A$. At first glance, the larger the probe

intensity the better, however if we check this expression carefully, we observe that the key factor is the energy density seen by the probe ray. Imagine that our probe ray is a very thin disk of area dS that moves at the speed of light. It scans a cylinder whose length is given by $c\tau_A$. Then $c\tau_A$ dS is the differential volume it covers and I_{0A} τ_A dS is the energy inside this volume. These differential volumes are shown in Fig. 18a for the case of counterpropagating lasers and in Fig. 18b for the case of crossing beams. In this second situation both probe and pump move in perpendicular directions, and the probe ray scans a region of the pump at a 45-degree angle due to the pump-probe relative motion. The region of the pump pulse scanned is indicated by the blue differential pencil. For this reason the ratio between the pump waist and its duration is relevant for the optimization of the nonlinearities. The shortest pump pulse not necessarily implies the strongest coupling (keeping constant the pump energy per shot).

In conclusion, to optimize the quantum vacuum nonlinearity it is necessary to maximize the energy inside this differential volume probed by the probe ray (blue lines in Fig. 18). This is important because it is not the intensity by itself what is relevant. For example, efforts to reduce the pulse duration converting a one PW pulse (30J/30fs) in a two PW pulse (30J/15fs) represent a great effort in enlarging the pulse bandwidth and do not help for our purpose. Pulses with a longer duration imply a smaller bandwidth and thus a smaller complexity than the OPA 15 fs or less available now. Extending the pump pulse duration is limited by the requirement that all its energy has to be at the waist at one. In other words the pump Rayleigh length has to be longer than the pulse length ($c\tau_A$), otherwise the pulse would have a complicated shape as shown in Fig. 19. This figure is a scheme for the case of $c\tau_A$ longer that the pump Rayleigh length. In this case the probe probes the pump before, during and after the pump waist. The overlapping that happens before or after the focus (right and left plot in Fig. 19) does not result in a relevant nonlinear effect because the pump intensity is far from its peak. Only the central part contributes.

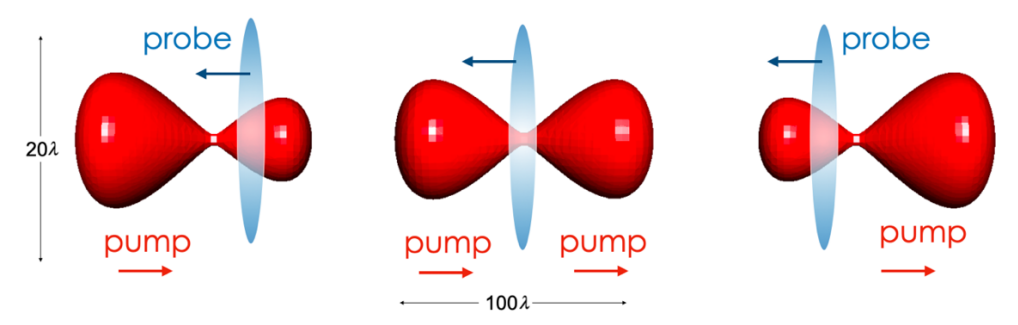


Figure 19.- Cartoon of the collision when the pump is a long pulse (300 fs in this case with a waist of only 2 μ m). Although this is just a drawing, the horizontal scale is compressed by a factor of 5 compared to the vertical scale to increase the visibility of the effect we want to show. If the pump pulse is too long not all its energy will be on the focal spot at the same time.

On the contrary, increasing the pulse duration helps to introduce more energy inside it. For this reason in the counterpropagating case a focus too tight is probably not the best option. The optimized pulse length is an interplay between the focal

number for the pump (not smaller that three certainly, and probably even longer) and the focal number of the probe, that has to be very high, indicating a wide focus.

As we mentioned before the infrared-infrared approach discussed here is not the only option to study quantum vacuum. There is an ongoing experiment in Hamburg's European XFEL where the pump is a PW-class laser and the probe is one of the XFEL X-ray beams. It is a counterpropagating geometry, to maximize the nonlinear n₂ coefficient. In that case the probe beam is the X-ray beam that is focused. With an extremely wide waist (wide in comparison to its wavelength) therefore the relation between waists and pulse lengths allows the use of a very long pulse. With this we would like to point out that the idea that, in order to maximize the nonlinearity, it is necessary to enhance the intensity as much as possible is not necessarily correct. An increase in the intensity is good if it increases the amount of energy "seen" by the probe ray. Or in other words, it is necessary to maximize the energy density inside the differential tube of section dS shown in Fig. 18. The present extreme lasers technology is saturating towards a limit of a few tens of PW [29]. Sometimes the increase of peak power is based on a reduction of the pulse duration keeping the pulse energy almost constant. This increases the peak intensity but does not optimize the energy density distribution, in fact some times it could even signify a slight decrease of the energy density seen by the probe ray.

9.- Conclusions

The quest of an experimental observation of the vacuum nonlinearities has not been successful for the moment [30, 31]. However lasers are improving performances very rapidly and a new generation of such experiments is expected using infrared-X-Ray or infrared-infrared [4].

In the previous Sections we analyzed two different configurations for a future infrared-infrared experiment that could solve the controversy between the Heisenberg-Euler and the Born-Infeld models. We can conclude that the geometrical factors appearing for different pump and probe configurations are not so different (compare 0.63 to 0.72), however the dependence of n_2 with the tilt angle (the angle between the two propagation vectors) is very relevant. There is a factor of 4 between the situations studied in Section 6 (counterpropagating) and in Section 7 (normal propagation vectors) and this is a fundamental effect that can not be avoided.

In these considerations we didn't include the longitudinal components of the field. Longitudinal fields are needed in order to fulfill the transversality conditions, $\nabla \cdot \mathbf{E} = 0$ and $\nabla \cdot \mathbf{B} = 0$ for the electric and magnetic fields. The transversality condition has been studied in many papers and there are very simple and convenient expressions to calculate them in first and second order [26]. For a wide waist probe, this longitudinal field is probably not going to be relevant. For the case of a pump focused with an f/3 parabola probably it is also negligible. However, for very tight focuses, close to f/1, longitudinal fields have to be included too. A visual

construction like the one shown in Fig. 14 probably will help to understand the effect of the Lagrangian couplings induced by such longitudinal fields.

Our objective has not been to produce a strong quantum vacuum effect. Our objective has been discussing situations where it is possible to have a clean and measurable quantum vacuum effect. For this reason, among other considerations, in this study we restricted ourselves to f/3 focal numbers in order to get clean results both for parallel and perpendicular polarizations. Our study indicates that reducing the focal number too much to get a very tight focus and trying to maximize the intensity is probably not the best strategy to maximize the quantum nonlinearity. To enhance the effect we are looking for, the parameter to maximize is the energy density distribution along the path of the central probe rays. This changes the refractive index seen by the probe ray and thus to enhances the probe diffraction, which is the signal we are looking for.

There is a need to keep these consideration in mind for the design of lasers specific to see these nonlinearities induced by the vacuum (or better by the virtual pairs present in vacuum). Some figures of merit typically used, such as the peak intensity, are relevant but not the only relevant specifications of the laser for this purpose. For example the optical quality of the probe pulse has to be as good as possible, with a Gaussian profile, to minimize its linear diffraction (diffraction with the pump off), and at the same time it has to be as intense as possible (signal proportional to the number of photons in the probe). Finally, it is relevant to mention that pump coherence, being relevant, is not as relevant as in other applications. A number of pump lasers, conveniently designed and finely synchronized, but incoherent between them, can be of interest for this application.

Therefore we are in front of a new generation of extreme laser experiments that requires tools specifically designed. At the same time new fundamental applications of such lasers are to be possible, in particular, ultraintense lasers as a tool to study dark matter.

These lines are dedicated to the memory of Professor Howard R. Reiss, an outstanding pioneer in extreme laser field physics, who taught some of us about those concepts.

Acknowledgements. This work was performed under the auspices of the U.S. Department of Energy by Lawrence Livermore National Laboratory under Contract No. DE-AC52-07NA27344, and the DOE Office of Science, Fusion Energy Sciences under Contract No. DE-SC0021231: the LaserNetUS initiative at The Scarlet Laser Facility. G.T, D.H, P.S, N.C, and R.D acknowledge support under Contract Nos. DE-SC0022092 and DE-SC0022094. R.F acknowledges support by the Natural Sciences and Engineering Research Council of Canada (Grant No. RGPIN-2019-05013). S.R, C.Z.H, N.M, and W.T.H acknowledge supported by the National Science Foundation (Grant No. PHY2308905). L.R, R.L, J.A.P-H, and J.I.A acknowledge support from Laserlab V (Grant Agreement No. 871124, European Union Horizon 2020 INFRAIA research and innovation program), from IMPULSE (Grant Agreement No. 871161, European Union Horizon 2020 INFRADEV research and innovation program), and from Junta de Castilla y León Grant No. CLP087U16.. J.A.P-H acknowledges support from the Spanish Ministerio de Ciencia e Innovación (Grant No PID2021-125389OA-I00, FEDER funded). R.L. and L.R. acknowledge support also from

the Spanish Ministerio de Ciencia e Innovación (Grants No PID2022-140593NB-C21 and -C22, respectively, both FEDER funded).

References

- D. Strickland, and G. Mourou. Compression of amplified chirped optical pulses. Optics Communications 55 (1985) 447
- G. Mourou. Extreme light physics and application. Reviews of Modern Physics 91, 030501 (2019)
- 3 Jin Woo Yoon et al. Realization of laser intensity over 1023 W/cm². Optica 8 630 (2021)
- 4 A. Fedotov et al. Advances in QED with intense background fields, Physics Reports 1010 (2023) 1
- 5 Qiqi Yu, et al. X-ray polarimetry and its application to strong-field QED. High Power Laser Science and Engineering. Accepted (2023).
- 6 F. Karbstein, et al. Direct accessibility of the fundamental constants governing light-by-light scattering. Physical Review Letters 129 (2022) 061802.
- 7 Kai S. Schulze, et al. Towards perfectly linearly polarized x-rays. Physical Review Research 4, 013220 (2022)
- 8 W. Heisenberg, and H. Euler. Folgerungen aus der Diracschen Theorie des Positrons. Zeitschrift für Physik 98 (1936) 714
- 9 M. Born, and L. Infeld. Foundations of the new field theory. Proceedings Royal Society London A 144 (1934) 425
- 10 Ch.D. Thomas. The scattering of light by light according to the Born-Infeld theory. Physical Review 50 (1936) 1046.
- 11 S. Robertson, Optical Kerr effect in vacuum, Physical Review A 100, 063831 (2019)
- 12 V.I. Ritus. Quantum effects of the interaction of elementary particles with an intense electromagnetic field. Journal of Soviet Laser Research 6 (1985) 497
- 13 H. Gies, and L. Roessler. Vacuum polarization tensor in inhomogeneous magnetic fields. Physical Review D 84 (2011) 065035
- 14 A. Di Piazza, et al. Reviews of Modern Physics 84 (2012) 1177
- 15 A. Ejlli, et al. The PVLAS experiment: A 25 year effort to measure vacuum magnetic birefringence. Physics Reports 871 (2020) 1
- 16 A. Arbey, and F. Mahmoudi. Dark matter and the early Universe: a review, Progress in Particle and Nuclear Physics 119 103865 (2021)
- 17 K.A. Beyer, G. Marocco, R. Bingham, and G. Gregori. Axion detection through resonant photon-photon collisions. Physical Review D 101 (2020) 095018.
- 18 H. Gies, F. Karbstein, and L. Klar, All-optical quantum vacuum signals in two-beam collisions. Physical Review D 106 (2022) 116005.
- 19 D. Tommasini, D. Novoa, and L. Roso. Quantum vacuum polarization searches with high power lasers below the pair production regime, in Progress in Ultrafast Intense Laser Science X Editors K. Yamanouchi G. G. Paulus, and D. Mathur. Springer Series in Chemical Physics 106 (2014) 137.
- 20 H.R. Reiss. Absorption of light by light. Journal of Mathematical Physics 3 (1962) 59.
- 21 C. Bamber et al. Studies of nonlinear QED in collisions of 46.6 GeV electrons with intense laser pulses. Physical Review D 60 (1999) 092004
- 22 P.J. Clark, et al. Measurement of the exclusive $\gamma\gamma \to \mu^+\mu^-$ process in proton-proton collisions at \sqrt{s} =13 TeV with the ATLAS detector. Physics Letters B 777 (2018) 303
- 23 S.I. Godunov, et al. LHC as a photon-photon collider: Bounds on Γ X \rightarrow γ γ . Physical Review D 103 (2021)035016
- 24 R. Karplus and M. Neuman. The Scattering of Light by Light. Physical Review 83, 776 (1951)
- 25 Yi Liang, and A. Czarnecki. Photon–photon scattering: a tutorial. Canadian Journal of Physics **90** (2012) 11
- 26 W.L. Erikson, and S. Singh. Polarization properties of Maxwell-Gaussian laser beams. Physical Review E 49 (1994) 5778
- 27 L. Roso, R. Lera, S. Ravichandran, A Longman, C.Z. He, J.A. Pérez-Hernández, J. Apiñaniz, L.D. Smith, R. Fedosejevs, and W.T. Hill, III. Towards a direct measurement of the quantum-vacuum Lagrangian coupling coefficients using two counterpropagating super-intense laser pulses. New Journal of Physics 24 (2022) 025010
- 28 R. Simon. Anisotropic Gaussian Beams. Optics Communications 46 (1983) 265
- 29 C.N. Danson, Petawatt and Exawatt Class Lasers Worldwide. High Power Laser Science and Engineering 7 (2019) e54
- 30 T. Inada, et al. Search for photon–photon elastic scattering in the X-ray region, Physics Letters B **732** (2014)
- 31 D. Bernard, et al. Search for stimulated photon-photon scattering in vacuum. European Physics Journal D 10 (2000) 141.